Space Sci Rev (2009) 149: 119–151
DOI 10.1007/s11214-009-9536-3

Quasi-Periodic Pulsations in Solar Flares

V.M. Nakariakov · V.F. Melnikov

Received: 26 January 2009 / Accepted: 7 May 2009 / Published online: 29 May 2009

Abstract Quasi-periodic pulsations (QPP) are a common feature of flaring energy releases in the solar atmosphere, observed in all bands, from radio to hard X-ray. In this review we concentrate on QPP with the periods longer than one second. Physical mechanisms responsible for the generation of long QPP split into two groups: "load/unload" mechanisms and MHD oscillations. Load/unload mechanisms are repetitive regimes of flaring energy releases by magnetic reconnection or by other means. MHD oscillations can affect all elements of the flaring emission generation: triggering of reconnection and modulation of its rate, acceleration and dynamics of non-thermal electrons, and physical conditions in the emitting plasmas. In the case of MHD oscillations, the periodicity of QPP is determined either by the presence of some resonances, e.g. standing modes of plasma structures, or by wave dispersion. Periods and other parameters of QPP are linked with properties of flaring plasmas and their morphology. Observational investigation of the QPP generation mechanisms based upon the use of spatial information, broadband spectral coverage and multi-periodicity is discussed.

Keywords Magnetohydrodynamics and plasmas · Flares · Magnetohydrodynamic waves · Magnetic reconnection

1 Introduction

One of the most remarkable achievements of solar physics in the last decade is the discovery of spatially-resolved magnetohydrodynamic (MHD) wave and oscillatory activity

V.M. Nakariakov (✉)
Physics Department, University of Warwick, Coventry CV4 7AL, UK
e-mail: V.Nakariakov@warwick.ac.uk

V.F. Melnikov
Central Astronomical Observatory at Pulkovo of the Russian Academy of Sciences, Saint-Petersburg 196140, Russia

V.F. Melnikov
Radiophysical Research Institute (NIRFI), Nizhny Novgorod 603950, Russia

of the corona (e.g. Nakariakov and Verwichte 2005). The observational evidence of MHD waves of various kinds in the corona is now abundant. Several theoretically predicted wave modes (transverse kink and sausage, and longitudinal) have been identified in the imaging and spectral data with high temporal and spatial resolution in the visible light, EUV, soft X-ray, and microwave bands. Characteristic periods of the MHD waves *directly detected in imaging observations* in solar coronal loops, plumes and other structures range from several seconds to several minutes. Most likely, this range is restricted by the parameters of the observational facilities, such as the cadence time, spatial resolution and duration of observational sequence. The amplitudes of the perturbations of MHD parameters: plasma density, bulk velocity, magnetic field, temperature, are rather small, typically less than several percents of the background. Thus, the presence of MHD waves and oscillations in the solar corona can now be taken as a unambiguously established fact. The interest to coronal waves and oscillations is mainly connected with the possible role played by them in the heating of the coronal plasma (e.g. Aschwanden 2004; Erdélyi and Ballai 2007), and with the use of them as natural probes for the plasma diagnostics (e.g. Nakariakov and Verwichte 2005; Banerjee et al. 2007).

The recent progress in the observational and theoretical study of coronal MHD waves stimulated the application of this gained knowledge to another example of oscillatory processes in the corona, the quasi-periodic pulsations (QPP) in flaring energy releases. QPP, with periods ranging from fractions of seconds (e.g. Aschwanden 1987; Fleishman et al. 2002; Tan 2008) to several minutes (e.g. Foullon et al. 2005; Kislyakov et al. 2006) are often observed in the light curves of solar flares. QPP can be present in both two-ribbon and compact types of flares. The modulation depth can reach 100% of the emission trend and can often be well recognised without data processing. The most pronounced QPP are seen in the emission associated with flare-accelerated non-thermal electrons in the microwave, hard X-ray and white light bands. QPP can be found in all stages of the flare, from pre-flaring to decaying phases. In the case of large modulation depth, the flare can be seen as a sequence of periodically separated bursts. Often, QPP are seen to be simultaneous and in phase in different bands, e.g. in hard X-ray and in microwave (e.g. Asai et al. 2001). A typical example of microwave and hard X-ray light curves generated by a solar flare with synchronous QPP observed in microwave and hard X-ray channels is shown in Fig. 1. Usually, in microwaves and hard X-rays, QPP are broadband features. Grigis and Benz (2004) investigated spectral evolution during individual peaks of the flaring hard X-ray emission and found each such subpeak to display a soft-hard-soft (SHS) evolution of the hard X-ray spectra. On the other hand, in microwaves we often see a soft-hard-harder (SHH) or even hard-soft-hard (HSH) evolution during each subpeak in the optically thin part of the frequency spectra (Melnikov and Magun 1998; Fleishman et al. 2008).

QPP can also be observed in subsequent flares occurring in the same active region (Grechnev et al. 2003). In some events, QPP have several significant periods (e.g. Melnikov et al. 2005; Kislyakov et al. 2006; Inglis and Nakariakov 2009). The periods of flaring QPP can be split into several bands. Aschwanden (2003) distinguished between very fast ($<$0.5 s), short period (0.5–5 s) and long period ($>$5 s). Possibly, a more practical, based on the possible interpretation, classification would be the separation between *short* (subsecond) QPP that usually have high quality, are detected in the radio emission and are likely to be associated with the interaction of EM, plasma or whistler waves with accelerated particles (see, e.g. Aschwanden 1987), and *long* QPP that usually have low quality, are detected in the microwave, white light, EUV and X-ray emission, and are likely to be associated with MHD processes. In this review, we concentrate our attention on the long, longer than

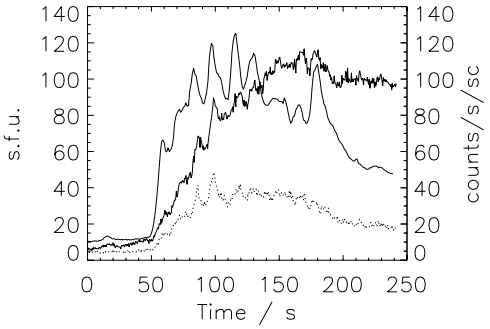

Fig. 1 Light curves of the flare on 1998 May 8 at 01:57 UT recorded with Nobeyama Radioheliograph in 17 GHz (*thick curve*) and with Yohkoh/HXT in the L (13–23 keV, *thin solid curve*) and M1 (23–33 keV, *dotted curve*) channels (from Inglis et al. 2008)

one second, QPP only. An online catalogue[1] of long QPP events summarises some known examples.

The interest to flaring QPP has several motivations. First of all, QPP are an intrinsic part of flares, and hence carry information about the mechanisms responsible for the energy releases, processes operating in them, and their triggering. From the point of view of coronal wave physics, flares are bright features and hence can be observed with high observational cadence time, down to fractions of a second. This allows for resolution of the wave transit time e.g. across magnetic plasma structures, which is important for various techniques of MHD coronal seismology. Moreover, the nearest vicinity of flare epicentres is the region of the corona where the likelihood of the excitation of waves and oscillations is highest. In addition, understanding of the relationship between QPP and the parameters of flaring plasma structures can contribute to the development of stellar coronal seismology, exploiting the similarity in structure and dynamics of the solar and Sun-like stellar coronae (Nakariakov 2007). The observational foundation of this novel approach is based upon QPP detected in stellar flares (e.g. Mathioudakis et al. 2003; Mitra-Kraev et al. 2005).

Theories describing long QPP in flares can be divided into two groups: load/unload models and oscillation models. The load/unload theories explain QPP as a side effect of transient energy releases, in particular of magnetic reconnection. The observed periodic behaviour is considered to be rather accidental, connected with the relationship between energy load and unload balance. This can be illustrated as a "drop" model: slowly and continuously leaking water is gathering on the ceiling, forming a bulge of growing mass, and when the gravitational force becomes sufficiently strong to counteract the surface tension force, the drop reconnects from the rest of the water and falls down. Then the situation repeats, and the drop rate can be quite periodic and stable. The period of drops is determined by the inflow rate, and the gravitational and surface tension forces. Similarly, in the case of magnetic reconnection, the magnetic energy can be continuously supplied by, e.g. photospheric motions, build up in the vicinity of a flare epicentre, and, when certain critical level of the magnetic field complexity is reached, the energy is released by a burst, and the buildup of the energy repeats again. This phenomenon is an example of an auto-oscillation, which is an AC resulting from the steady supplied energy (DC).

On the other hand, oscillation theories link the observed periodicity with the modulation by MHD oscillations or waves of some elements of the chain leading to flaring emission: the rate of the energy release, including triggering the reconnection, conditions of particle acceleration and/or injection, particle dynamics, and parameters of the emitting plasma. The

[1] http://www2.warwick.ac.uk/fac/sci/physics/research/cfsa/people/valery/research/qpp.

periodicity is prescribed either by certain resonances or by dispersive narrowing of initially broad spectra.

There is another group of theories developed for the explanation of QPP, based upon the oscillatory regimes of the nonlinear interaction of electro-magnetic (EM), whistler, ion-acoustic or plasma waves with each other and with accelerated electrons (see, for detailed review Aschwanden 1987; Zaitsev and Stepanov 2008). One of the examples of such theories is the approach based upon the equations of the Lotka–Volterra type (Zaitsev 1971). The period of such QPP is mostly determined by plasma wave damping due to collisions of thermal electrons with ions. For the typical conditions in flaring loops, it is very small, of order tens of milliseconds. Similar formalism was developed by Aschwanden and Benz (1988) for the electron cyclotron maser phenomenon. These mechanisms are applicable to the interpretation of fast QPP, but they are not likely to produce longer periods, and hence are out of scope of this review.

At present, observational data do not permit an unambiguous choice between various models for flaring QPP. Also, it is quite likely that in different cases operate different mechanisms or their combinations. In this review, we consider physical mechanisms for the generation of flaring QPP with the periods longer than one second, the relation of periods with physical parameters of the flaring systems, and recent attempts to determine the mechanisms responsible for the observed QPP. In Sect. 2 we discuss the generation of QPP by periodic regimes of magnetic reconnection. In Sect. 3 we briefly review hydrodynamic oscillations connected with thermal over-stability. Section 4 describes QPP produced by MHD waves and oscillations, including standing and propagating modes, the LCR-contour model, ballooning and kink over-stabilities, and mechanisms for the modulation of the emission in different bands by MHD waves, and the external triggering of periodic magnetic reconnection. In the following sections we consider the recent approaches to the determination of the mechanisms responsible for QPP: Sect. 5 discusses the use of the spatial information, events with several significant periodicities are reviewed in Sect. 6, and the use of spectral resolution is presented in Sect. 7. The progress in the theoretical and observational studies of flaring QPP is summarised in Conclusions.

2 Oscillations Generated by Magnetic Reconnection

As a complex, highly nonlinear, threshold-depending process, magnetic reconnection can operate in different regimes, in particular, oscillatory. Indeed, dynamic models of magnetic reconnection predict that the processes of tearing instability and coalescence of magnetic islands occur repetitively, leading to an intermittent or impulsive bursty energy release and particle acceleration.

Kliem et al. (2000) simulated numerically the evolution of a long current sheet above a soft X-ray loop. The geometry was consistent with the 2D Carmichael–Sturrock–Hirayama–Kopp–Pneuman (CSHKP) model of a flare. In the simulations, resistivity was anomalous and determined self-consistently from the electron-ion drift velocity, proportional to the electric current density. The positive feedback between reconnection, plasma acceleration and rise of the resistivity resulted in self-sustaining reconnection with variable rate. More specifically, resistive magnetic reconnection of the current sheet was found to operate in a time-variable manner, involving repeated generation of magnetic islands and their coalescence. The principle effect that leads to the variable regime of reconnection (in contrast with the steady regime) is the inability of the plasma to carry a sufficient amount of magnetic flux into the diffusion region to support the Alfvénic outflow in steady Petchek

state. Thus the system kept switching between Petchek and Sweet–Parker regimes of reconnection. The formation of each new island was suggested to be accompanied with a burst of accelerated particles and hence a pulsation of the observed emission in all bands associated with non-thermal electrons: hard X-ray, microwave, decimeter, meter. The repetitive precipitation of the accelerated electrons would also induce repetitive upflows of hot plasma and hence produce the modulation of the soft X-ray emission. The pulsations repeat at the rate

$$P_R \propto n_0^{-1/2} T_0^2 B_0^{-1} \tag{1}$$

determined by the plasma concentration n_0, temperature T_0 and magnetic field B_0 outside the current sheet, respectively. The repetition rate was found to be about thirteen Alfvén crossing times between neighbouring X-points in the generated sequence of plasmoids. For the plasma concentrations in the range 10^9–10^{10} cm^{-3}, the time between pulsations could be 0.4–20 s. Kliem et al. (2000) concluded that this mechanism could explain the occurrence of irregular or quasi-periodic pulsations with timescales in this range.

The tearing mode instability of a current sheet can be modified in the presence of sufficiently fast shear flows. 2.5D compressive, visco-resistive MHD simulations of the flare model proposed by Heyvaerts et al. (1977), performed by Ofman and Sui (2006), demonstrated that field-aligned shear flows or beams with super-Alfvénic speeds in the vicinity of current layers lead to the coupling of tearing mode and Kelvin–Helmholtz instabilities. The coupling can result in appearance of overstable (i.e., oscillating) modes. This effect is most pronounced if plasma β (which is the ratio of the thermodynamic and magnetic pressures) is greater than unity, which may be achieved in flares (see, e.g. Shibasaki 2001). It was suggested that the observed non-thermal X-ray emission oscillations are due to variations of the electric current magnitude in the reconnection region, induced by the overstable coupled tearing and Kelvin–Helmholtz modes induced by Alfveńic or super-Alfveńic flows and beams. The current fluctuations affect the electric field magnitude and, consequently, modulate the electron acceleration rate. In the simulations, the period of oscillations was found to be about 50 Alfvén transit times across the current sheet half-width.

Oscillatory regimes of nonlinear coalescence instability in a system of current carrying (twisted) loops, demonstrated by Tajima et al. (1987), can be also attributed to this group of mechanisms. In this model the governing equation describing the time evolution of the magnetic field in the current sheet formed by collision of two loops is

$$\ddot{\zeta} = -\zeta^{-2} + \beta\zeta^{-3}, \tag{2}$$

where ζ is a dimensionless parameter connected with the magnetic field strength, $B \propto \zeta^{-2} x/w$, with x being a coordinate across the sheet and w being its width, and the time is measured in Alfvén transit times across the current sheet. Numerical solutions to (2) are shown in Fig. 2. The solid curve corresponds to $\dot{\zeta}(0) = 1$, the dotted curve to $\dot{\zeta}(0) = 0.5$, and the dashed curve to $\dot{\zeta}(0) = 0$. The magnetic field experiences periodic spikes, causing periodic spikes of the current density. The minimal period of these oscillations is

$$P_{\text{coal}} = 2\pi \frac{C_s^3 \varepsilon}{C_A^4}, \tag{3}$$

where C_s and C_A are the sound and Alfvén speeds, respectively, and ε is characteristic length of the interaction region, connected in this case with the width of the current sheet formed at the boundary between the interacting twisted loops. More generally, the period also depends upon the plasma β, the magnetic twist (the ratio between the poloidal and

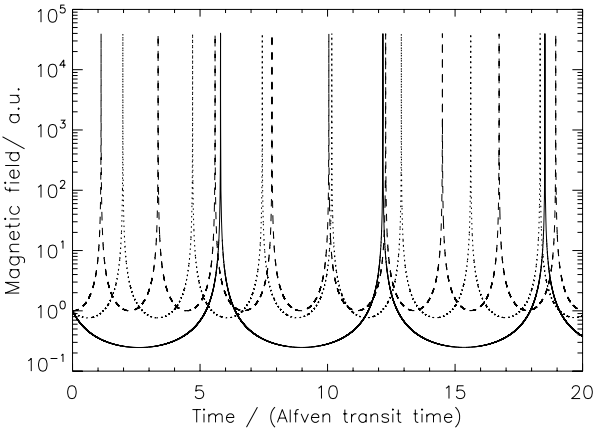

Fig. 2 Magnetic field variations across the current sheet in Tajima et al. (1987) model of coalescence instability of current carrying loops. The time is measured in Alfvén transit times across the current sheet. Different *curves* correspond to different initial rates of the field evolution

toroidal components of the field in the loops), and on the colliding velocity of the loops. According to numerical simulations, the oscillations can have double or triple sub-peaks, which is consistent with some observational examples of QPP (e.g. see Fig. 1 in Kane et al. 1983). These oscillations are essentially nonlinear, and their period is connected with the amplitude (Fig. 2) or the dynamic range of the current variation. Both period and amplitude depend strongly upon the initial conditions. The electrostatic field was found to grow in the explosive phase more rapidly than the magnetic field, which results in efficient acceleration of particles.

Recently, oscillatory regimes of magnetic reconnection were studied numerically in frames of 2.5D MHD by Murray et al. (2009). A flux rope emerged into the solar atmosphere endowed with a vertical magnetic field, which represented a coronal hole region. A current sheet readily built along a side interface between the expanding emerged loops and the neighbouring coronal hole field, where the magnetic fields were of opposite orientation. Interchange reconnection set in and generated new closed loops and new open field with footpoints near the emerged loops. It was found that a series of reconnection reversals took place, whereby reconnection occurred in distinct bursts and the inflow and outflow magnetic fields of one burst of reconnection became the outflow and inflow fields in the following burst of reconnection, respectively. During each burst of reconnection the gas pressure in the bounded outflow regions increased above the level of that in the inflow regions and, eventually, gave rise to a reconnection reversal. Oscillatory reconnection was found to cause periodic changes in the maximum current and heating in the current sheet, and that the largest maximum values in each phase reduce with time. The oscillation periods observed in the simulations of Murray et al. (2009) ranged from 1.5 min to 32.1 min (see Fig. 3). Numerical resistivity in these simulations was much higher than physical resistivity, but, providing the reconnection proceeds sufficiently fast so that the system overshoots the equilibrium point, oscillatory reconnection is expected to set in anyway. However, modification of the resistivity value can alter the value of the reconnection rate and the period of the oscillations.

The advantage of the QPP generating mechanisms based upon time-dependent magnetic reconnection is that these models naturally explain the simultaneity of the oscillations in different bands, as they are produced by the same cause: the time-varying rate of the electron acceleration. Also, the deep modulation depth of QPP is easily given by these mechanisms, as it is determined by the variations of non-thermal electron density. However, it is not clear whether time-dependent reconnection can explain the high monochromaticity and quality

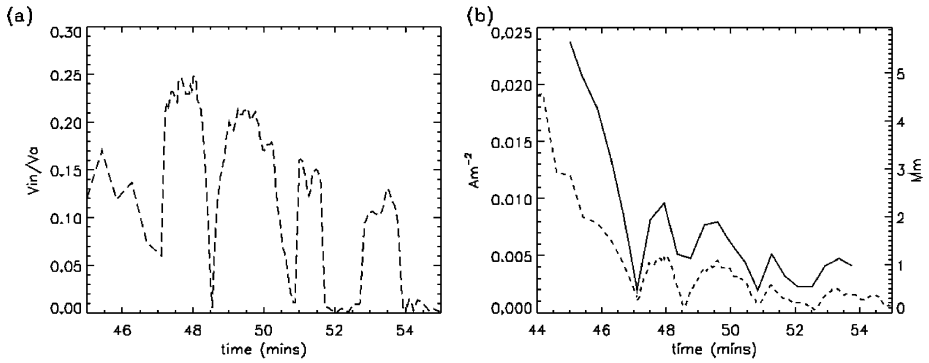

Fig. 3 Spontaneous periodic reconnection in the emerging magnetic flux in a coronal hole. *Left panel:* Reconnection rate given by the inflow Alfvén Mach number. *Right panel:* maximum current in the current sheet (*dashed*), measured in units of Am^{-2}, and length of the current sheet (*solid*), measured in units of Mm, as functions of time (from Murray et al. 2009)

of oscillations and presence of several significant periodicities, sometimes detected in flaring light curves. Also, the properties of the non-thermal electron energy spectra produced by those mechanisms are still to be revealed. In particular, it would be interesting to know whether the models reproduce the observables associated with the non-thermal electron dynamics: have the generated the spectra power-law shape, and whether the time variation of the non-thermal electron concentration is accompanied by variation of the spectral index.

3 Thermal Over-Stability

The imbalance of the plasma heating and energy losses caused by optically thin radiation and thermal conduction can lead to the periodic variations of MHD parameters of plasmas, known as thermal over-stability. Consider a simplified model of this phenomenon restricting our attention to the field-aligned processes only, and neglecting induced variations in the magnetic field. Kuin and Martens (1982) derived a set of coupled nonlinear ordinary differential equations (ODE) describing the time evolution of the normalised density $\bar{n}$ and temperature $\bar{T}$ in a coronal loop filled by a hot plasma under the assumption that the heating function was constant per unit volume,

$$\frac{\mathrm{d}\bar{T}}{\mathrm{d}\bar{t}} = \frac{1}{\bar{n}}\left[1 - \bar{n}^2\Psi(\bar{T}) - \Upsilon(\bar{T}-1)\right], \tag{4}$$

$$\frac{\mathrm{d}\bar{n}}{\mathrm{d}\bar{t}} = \Gamma\Upsilon(1 - \bar{T}^{-1}), \tag{5}$$

where the time $\bar{t}$ is measured in units which depend upon the equilibrium, Υ is a dimensionless constant determined by equilibrium, and Γ $(0 \le \Gamma \le 1)$ is another dimensionless constant which determines the chromospheric evaporation efficiency. Numerical investigation of (4)–(5) demonstrated the existence of a limit cycle solution which corresponds to stable nonlinear oscillations of the temperature and density with the period longer than the acoustic transit time in the loop.

The possibility of the thermally over-stable dynamical regimes in coronal loops with time-independent nonuniform heating was confirmed by the hydrodynamic numerical simulations performed by Müller et al. (2004). A periodic variation of the loop temperature and

density due to the evaporation-condensation cycle, accompanied by subsonic longitudinal flows of matter along the loop, was found. Parametric studies demonstrated the existence of the limit cycle regime.

The periods studied by Kuin and Martens (1982) and by Müller et al. (2004) are several hours, however shorter period regimes could exist too. Nakariakov et al. (2004) numerically modelled the response of a coronal loop to an impulsive spatially localised heat deposition and found decayless compressible oscillations corresponding to the second spatial harmonics of the longitudinal (also called acoustic) mode (see also Sect. 4.2 and (13)). It was concluded that regime corresponded to an auto-oscillation[2], with the thermally unstable plasma playing the role of an active medium. Detailed numerical parametric studies of this phenomenon in Tsiklauri et al. (2004) showed that the second spatial harmonics of the longitudinal mode is a robust feature of an impulsively heated coronal loop.

The periodic variation of the hydrodynamic parameters in the loop can modulate the energy release in the flare (see Sect. 4.5) or the emission from the flaring loop (Sect. 4.4), and hence be present in hard X-ray, white light and microwave light curves.

4 Mechanisms Based upon MHD Oscillations

Large scale (much greater than ion gyroradii) and slow (with characteristic times much longer than ion gyro-period) dynamics of magnetised plasmas are adequately described by magnetohydrodynamics. The set of MHD equations links the macroscopic parameters of the plasma: mass and current densities, temperature, gas pressure, bulk flow velocities, and the magnetic field. Variation of these quantities in the vicinity of flare sites can affect flaring emission.

4.1 MHD Modes of Plasma Cylinders

The standard model for the study of linear MHD modes of coronal structures is interaction of MHD waves with a plasma cylinder which reproduces the main properties of loops, jets, filaments, and other approximately axially symmetric coronal structures. In the model, the equilibrium MHD plasma parameters, such as density, magnetic field and gas pressure experience a jump at the cylinder boundary ($r = a$) which can be considered to be discontinuous. The equilibrium is determined by the total pressure balance at the boundary. In the internal and external media, the sound speeds are C_{s0} and C_{se}, and the Alfvén speeds are C_{A0} and C_{Ae}, respectively. For slow magnetoacoustic waves, it is convenient to introduce the tube (or cusp) speeds C_{T0} and C_{Te}, where $C_{T0,e} = C_{s0,e}C_{A0,e}/\sqrt{C_{s0,e}^2 + C_{A0,e}^2}$. Ratios between those characteristic speeds prescribe properties of MHD modes guided by the tube. The formalism for the determination of MHD modes of this structure and for the derivation of their dispersion relations was developed by Zaitsev and Stepanov (1975) and by Edwin and Roberts (1983).

The longitudinal wave number k_z (along the cylinder axis), the azimuthal wave number m, and the frequency ω are connected with each other by the dispersion relation

$$\rho_e(\omega^2 - k_z^2 C_{Ae}^2)m_0 \frac{I_m'(m_0 a)}{I_m(m_0 a)} + \rho_0(k_z^2 C_{A0}^2 - \omega^2)m_e \frac{K_m'(m_e a)}{K_m(m_e a)} = 0, \tag{6}$$

[2] An auto-oscillation is an undamped periodic process in a nonlinear dynamical system with the amplitude and period largely independent of the initial conditions, and determined by the properties of the system itself. Examples of auto-oscillators are clocks, bow and blow musical instruments, aerodynamic flutter, etc.

where $I_m(x)$ and $K_m(x)$ are modified Bessel functions of order m, and the prime denotes the derivative with respect to argument x. Functions m_0 and m_e which may be considered as radial wave numbers of the perturbations inside and outside the cylinder, respectively, are defined as

$$m_i^2 = \frac{(k_z^2 C_{si}^2 - \omega^2)(k_z^2 C_{Ai}^2 - \omega^2)}{(C_{si}^2 + C_{Ai}^2)(k_z^2 C_{Ti}^2 - \omega^2)}, \tag{7}$$

where $i = 0, e$, the indices stand for the internal and external media, respectively. For modes that are confined to the tube (evanescent outside, in $r > a$), the condition $m_e^2 > 0$ has to be fulfilled. The choice of the modified Bessel functions $K_m(x)$ for the external solution is connected with the demand of the sufficiently fast, exponential evanescence of the solution outside the loop (such perturbations are known as trapped or guided modes). In the typical coronal conditions, the waveguiding plasma structure is of higher density with respect to the external medium, and the plasma is of low β. Phase speeds of the trapped modes form two bands, from C_{T0} to C_{s0}, and from C_{A0} to C_{Ae}, corresponding to the *slow* and *fast* modes, respectively. The slow modes are essentially longitudinal, propagate at the speed close to the sound speed inside the cylinder, and can be considered as modified acoustic waves. In coronal conditions, slow modes are weakly dispersive, in contrast with fast waves which can be highly dispersive. Typical plots of the dispersion showing the real phase speed solutions of dispersion relation (6) can be found in Edwin and Roberts (1983), Nakariakov and Verwichte (2005) and Nakariakov (2007).

There are also essentially incompressible dispersionless *torsional* waves in the cylinder. They are propagating twists of the cylinder, moving the plasma in the direction locally parallel to the boundary of the cylinder. Each torsional wave is situated at a certain magnetic surface and propagate at the Alfvén speed. Torsional waves perturbing neighbouring magnetic surfaces do not interact with each other, hence they cannot be considered as collective modes. If there is an Alfvén speed gradient across the magnetic field, torsional waves are subject to phase mixing. This mode is the only one which can be considered as an Alfvén wave. Despite a number of recent claims, true Alfvén waves have not been detected in the corona yet.

The integer m, the azimuthal mode number, determines the azimuthal modal structure: waves with $m = 0$ are *sausage* (also known as radial, fast magnetoacoustic, peristaltic) modes, waves with $m = 1$ are *kink* modes, waves with $m > 2$ are referred to as *flute* or ballooning modes. For $m_0^2 < 0$, the internal radial structure of the modes is described by the Bessel functions $J_m(x)$, and the radial dependence of the oscillation inside the cylinder is quasi-periodic. The radial number l is connected with the number of oscillation maxima in the cylinder in the radial direction. There is an infinite number of modes with a given azimuthal number m, corresponding to different radial numbers l. The fast modes with higher radial numbers l have higher phase speeds along the loop and exist for higher values of the longitudinal wave number k_z. For standing modes, the boundary conditions in the longitudinal direction lead to the quantisation of the longitudinal wave number k_z, introducing a longitudinal number n which is an integer corresponding to the number of maxima of the transverse velocity perturbations along the loop. The modes with the lowest value of the longitudinal number, $n = 1$, which have wavelength equal to double the length of the resonator, are called *global* or fundamental (also known as principal).

Thus, dispersion relation (6) allows us to determine the frequency of a trapped magnetoacoustic mode if the three integer mode numbers (the longitudinal number n, the radial number l and the azimuthal number m) are given. The existence and properties of these modes are determined by the equilibrium physical quantities. The efficiency of their excitation depends upon the temporal-spatial spectrum of the driver or initial perturbation.

4.2 Typical Periods of Standing Waves

According to the previous section, there are four main MHD modes in a coronal loop or another cylindrical plasma structure: the sausage, kink, longitudinal and torsional modes. Sausage modes ($m = 0$) are perturbations of the loop minor radius, accompanied, because of the frozen-in condition, by the perturbations of the plasma density and the absolute value of the field. Kink modes ($m = 1$) are displacements of the axis of the loop. Kink modes are weakly compressible and are sometimes confused with Alfvén waves. Longitudinal modes are variations of the density of plasma and flows along the magnetic field, resembling the acoustic waves. Longitudinal waves of different m have almost indistinguishable properties. Sausage, kink and longitudinal modes are magnetoacoustic waves, as they are compressible, dispersive and collective. Torsional modes are oscillating or propagating twists of the magnetic field, associated with the alternate currents along the axis of the structure, incompressible and are subject to phase mixing: neighbouring magnetic surfaces oscillate independently of each other. The longest period modes of each kind, with the wavelength equal to double the loop length, are the global modes.

The period $P_{\rm saus}$ of the *global sausage mode* of a coronal loop is

$$P_{\rm saus} = 2L/C_{\rm p}, \tag{8}$$

where L is the length of the loop, $C_{\rm p}$ is the phase speed of the sausage mode corresponding to the wave number $k_z = \pi/L$, which is in the range $C_{\rm A0} < C_{\rm p} < C_{\rm Ae}$. The sausage mode has a long wavelength cutoff given by the critical wave number

$$k_{zc} \approx \frac{2.40}{a}\left[\frac{(C_{s0}^2 + C_{A0}^2)(C_{Ae}^2 - C_{T0}^2)}{(C_{Ae}^2 - C_{A0}^2)(C_{Ae}^2 - C_{s0}^2)}\right]^{1/2}. \tag{9}$$

Trapped sausage modes can exist only if their longitudinal wave numbers are greater than the cutoff value. For $k_z \to k_{zc}$, $C_{\rm p}$ tends to $C_{\rm Ae}$ from below, and for $k_z \to \infty$, $C_{\rm p}$ tends to $C_{\rm A0}$ from above. Thus, for long and thin loops, there are no trapped global sausage modes. However, there can be leaky global sausage modes in such loops with the phase speeds approximately equal to the external Alfvén speed (Pascoe et al. 2007). Figure 4 shows results of full MHD numerical simulations of the global sausage mode in a flaring coronal loop modelled as a straight slab of a low-β plasma with the symmetric Epstein profile of the plasma density. In all simulations the loop semi-width was $a = 3$ Mm. The density contrast ratio varied as $\rho_0/\rho_e = 2$, 5 and 10. For these density ratios, the loop lengths $L_c = 2\pi/k_{zc}$ above which the global sausage mode becomes leaky are 6.66 Mm, 13.33 Mm, and 19.99 Mm respectively. The corresponding values of the internal Alfvén speed were $C_{A0} = 2.12$ Mm s^{-1}, 1.34 Mm s^{-1} and 0.95 Mm s^{-1}, respectively. In all runs, the external Alfvén speed was kept the same, $C_{Ae} = 3$ Mm s^{-1}. For each density contrast ratio, simulations were performed for loop lengths between $L = 9$ Mm and $L = 60$ Mm. Thus, the wave length of the global sausage mode could be either shorter or longer than the cut-off wave length, covering both trapped and leaky regimes, respectively. According to the left panel of Fig. 4, in the trapped regime, periods of excited global sausage modes coincide with the periods calculated with the use of the analytical dispersion relation. For longer periods, in the leaky regime, the period depends upon the length of the loop almost linearly, and can be approximated by the expression

$$P_{\rm leaky} \approx 2L/C_{Ae}. \tag{10}$$

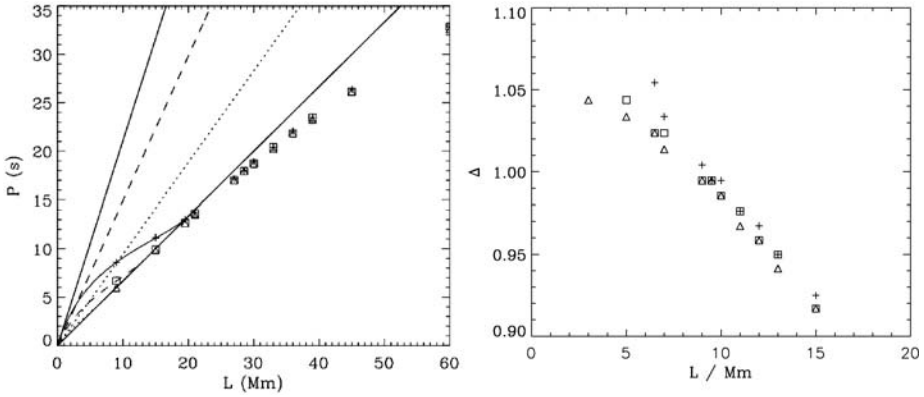

Fig. 4 *Left panel:* The dependence of the period of global sausage oscillation upon the loop length L for density contrast ratios of 2 (*triangle*), 5 (*square*) and 10 (*cross*). *The dotted*, *dashed* and *solid curved lines* correspond to the analytical dispersion relations for density contrast ratios of 2, 5 and 10 respectively. *The lower solid line* corresponds to a period of $2L/C_{Ae}$. *The dotted, dashed and upper solid lines* correspond to the values of $2L/C_{A0}$ for density contrast ratios of 2, 5 and 10 respectively. *Right panel:* The dependence upon the loop length of the difference Δ between the numerically obtained period and the period estimated using the external Alfvén speed, $2L/C_{Ae}$ The symbols corresponding to different density contrast ratios are the same as in *the left panel* (from Pascoe et al. 2007)

The difference between the values of periods calculated numerically and by expression (10) is shown in the right panel of Fig. 4. This difference is less than 10%, and hence expression (10) gives us a very good approximation for the estimation of the period of the global sausage mode in the leaky regime.

The period of the *global kink mode* is

$$P_{\text{kink}} = 2L/C_k, \tag{11}$$

where the kink speed

$$C_k \approx \left(\frac{2}{1+\rho_e/\rho_0}\right)^{1/2} C_{A0}. \tag{12}$$

In typical coronal conditions, the kink speed is slightly, by a about a factor of 1.4, higher than the Alfvén speed inside the loop. As with any transverse mode, the kink mode can have either vertical or horizontal polarisation (corresponding to a superposition of LH or RH circular polarisations, $m = \pm 1$), or be their combination. In the cylinder model, both these polarisations have the same phase speed, so the same oscillation period. The phase speeds of vertically and transversely polarised kink modes of curved loops are quite close to each other (Van Doorsselaere et al. 2004), which justifies the use of the cylinder model.

The period of the *global longitudinal mode* is given by the expression

$$P_{\text{long}} = 2L/C_{T0}. \tag{13}$$

In the low-β plasma typical for coronal conditions, the internal tube speed C_{T0} is very close to the internal sound speed C_{s0}, hence the period P_{long} is practically determined by the temperature in the loop and should evolve together with it. For higher values of β, perturbations of the magnetic field in the longitudinal mode become significant.

The resonant period of the *global torsional mode* is

$$P_{\rm tors} = 2L/C_{A0}. \tag{14}$$

This mode is purely internal and contains no information about the external medium. If the Alfvén speed varies in the radial direction, each cylindrical magnetic surface oscillate with its own period.

4.3 Propagating Fast Wave Trains

According to dispersion relation (6), in contrast with the torsional mode, all magnetoacoustic modes of plasma structures are dispersive, their phase and group speeds depend upon the frequencies and wave numbers. This dispersion is known as "geometrical", and appears because of the presence of a characteristic spatial scale in the system: e.g. the width of the loop, correlation length of random structuring, localisation length of the trapped wave near the guiding structure. Fast magnetoacoustic modes with wave lengths comparable to the characteristic scale of structuring can be highly dispersive. For example, in the long wavelength limit $k_z a \ll 1$, the kink mode of a plasma cylinder has the phase speed given by the expression

$$\omega/k_z \approx C_k\left[1 - \frac{\rho_0\rho_e}{2(\rho_0+\rho_e)}\frac{(C_{Ae}^2 - C_{A0}^2)}{(\rho_0 C_{A0}^2 + \rho_e C_{Ae}^2)}(k_z a)^2 K_0(|k_z|a)\right] \tag{15}$$

where the kink speed C_k is given by expression (12) and $K_0(x)$ is the modified Bessel function of the zero-order (Edwin and Roberts 1983). For small arguments $K_0(x)$ behaves like $-\log x$. Sausage and ballooning modes are even more dispersive, while longitudinal modes are weakly dispersive.

Because of dispersion, different spectral components of the wave propagate at different speeds. This leads to the evolution of an initially broadband perturbation to a quasi-periodic signal. Locally, the signal can look almost monochromatic, but at different instants of time the period of oscillations is different—the signal becomes frequency modulated. Also, the signal can have pronounced amplitude modulation, as, initially, different spectral components have different energy. In addition, the amplitude modulation can occur because of frequency-dependent dissipation and wave leakage. All above is applicable to fast magnetoacoustic waves guided by coronal plasma structures, e.g. loops, filaments, etc. Hence, impulsively excited propagating MHD perturbations develop into quasi-periodic wave trains.

Studying the dispersive evolution of propagating sausage modes of a straight magnetic cylinder, Roberts et al. (1984) qualitatively predicted that the signal develops into a quasi-periodic wave train. The characteristic feature of such a wave train is the presence of three distinct phases: the periodic phase, the quasi-periodic phase, when the signal has frequency modulation, and the decay phase. The highest amplitude of the signal is reached during the quasi-periodic phase which duration is $z(1/\min\{V_g\} - 1/C_{A0})$, where z is the distance from the point of the observation to the location of the initial excitation, and $\min\{V_g\}$ is the minimum group speed of the mode, which is less than C_{A0}. Such an evolution scenario is determined by the presence of a minimum in the group speed dependence upon the wave number. An estimation of the characteristic period, derived in Roberts et al. (1984), is

$$P_{\rm prop} \approx \frac{2\pi w}{j_0 C_{A0}}\sqrt{1 - \frac{\rho_e}{\rho_0}}, \tag{16}$$

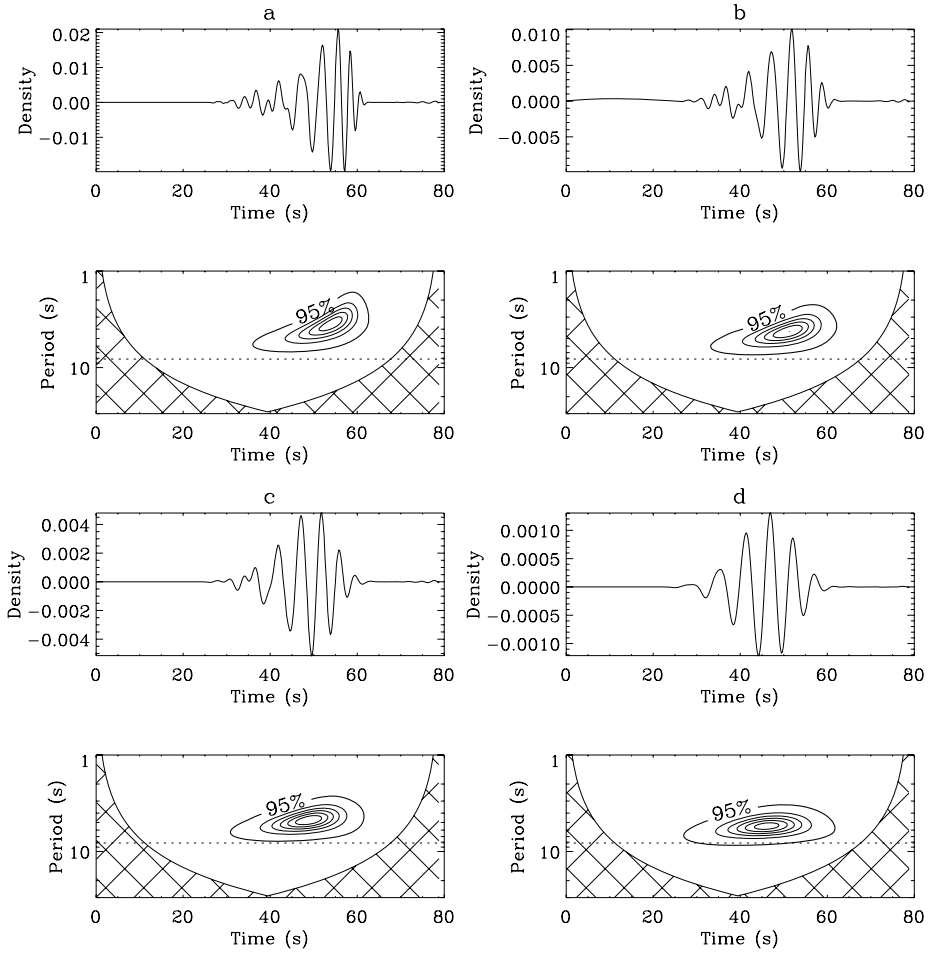

Fig. 5 Density perturbations in impulsively generated fast wave trains of sausage symmetry in a plasma slab, and their wavelet transforms, for different longitudinal localisation λ_z of initial perturbation of Gaussian shape: (**a**) $\lambda_z = w/2$, (**b**) $\lambda_z = w$, (**c**) $\lambda_z = 3w/2$, (**d**) $\lambda_z = 5w/2$, where w is the slab half-width. *The horizontal dotted line* shows the value of the longest possible period of a guided sausage mode, which in the considered waveguide is 8.2 s (from Nakariakov et al. 2005)

where w is the slab half-width, and $j_0 \approx 2.40$ is the first zero of the Bessel function $J_0(x)$. In loops with the large contrast ratio $\rho_e \ll \rho_0$, (16) reduces to $P_{\text{prop}} \approx 2.6w/C_{A0}$. The typical periods are close to the transverse Alfvén transit time, and hence the mean wave length is about the width of the structure. We would like to point out that expression (16) provides us only with the estimation of the range of the periods, as the intrinsic feature of the discussed effect is the variation of the period with time. Wave trains with signatures qualitatively similar to the theoretically predicted were found in 303 and 343 MHz coronal data recorded by the Icarus radio spectrometer (Roberts et al. 1984).

Full MHD numerical simulations of the dispersive evolution of a fast wave train, propagating along the magnetic field in a low-β plasma slab (Nakariakov et al. 2004) confirmed the qualitative prediction that development of an impulsively generated pulse leads to the

formation of a quasi-periodic wave train with the mean wavelength comparable with the slab width. In agreement with the analytical theory, wave trains have a pronounced period and amplitude modulation, which suggests the use of the wavelet transform technique as a convenient analytical tool. It was found that the dispersive evolution of fast wave trains leads to the appearance of characteristic "tadpole" wavelet signatures: the wave train amplitude is gradually growing while the period decreases (shown in Fig. 5). This wavelet spectral signature is a robust feature of this effect. Perhaps, such a signature should be rather called a "crazy tadpole", as it comes tail-first. Similar wavelet signatures were found in the propagating 6-s wave trains detected during solar eclipses (Nakariakov et al. 2004).

The width of Fourier or global wavelet spectra of a dispersively formed fast wave train are determined by the parameters of the waveguide: the density contrast, the steepness of the Alfvén speed profile, and plasma-β. For the sausage mode, the resultant spectra are also determined by distribution of the initial spectrum with respect to the cut-off. The spectral part which corresponds to the leaky regime radiates out of the waveguide, and the guided energy can then be quite monochromatic, as was demonstrated in Nakariakov et al. (2005). Figure 5 presents results of numerical modelling of fast sausage wave trains formed at a certain distance (approximately 15 slab widths) from the location of an impulsive energy deposition in a low-β plasma slab. The transverse profile of the density was smooth, given by the symmetric Epstein function. The ratio of the density at the slab top to the background equals to 5. The initial perturbation is of Gaussian shape, localised along and across the slab. The initial perturbation was chosen to be symmetric, so only sausage modes were excited. Different panels of Fig. 5 demonstrate the wave trains developed from the initial Gaussian perturbations of different longitudinal widths, and their wavelet spectra. Apparently, in all cases, the energy of the wave trains has periods shorter than the cut-off period of the guided sausage mode. The spectral components with the periods longer than the cut-off value leak out the slab very efficiently and are not present in the spectrum of the guided wave trains at all. It is also evident that the wave trains generated by longer initial pulses have less pronounced "crazy tadpole" spectral signatures and are more monochromatic.

The periods of dispersively formed fast wave trains should be significantly shorter than the longitudinal length of the guiding structures, otherwise the impulsive excitation generates standing modes discussed in Sect. 4.2. Then, as in typical coronal conditions the longitudinal transit time is significantly longer than the transverse transit time, the typical periods of the wave trains formed by the dispersion are about a few s.

4.4 Modulation of Flaring Emission by MHD Modes

The most suitable band for the study of the variation of macroscopic parameters of flaring plasmas by MHD waves is the microwave band, as modern microwave observational tools are ground-based, have excellent time resolution and sensitivity, and in the case of radioheliographs, spatial resolution. In some cases spectral resolution is also available.

Consider modulation of the microwave emission produced by mildly relativistic electrons accelerated in solar flares, by MHD waves via the gyrosynchrotron mechanism. Gyrosynchrotron emission is caused by the interaction of non-thermal particles with a background magnetic field. Generally, the gyrosynchrotron emission I_f at a fixed frequency f is determined by the total number of non-thermal electrons in the emitting volume (usually, the electrons with energies higher than some certain threshold value, e.g. 10 keV, are taken into account), the angle θ between the line-of-sight (LOS) and the magnetic field, the absolute value of the magnetic field B, the plasma concentration n_0 and the energy power law index δ (usually $\delta > 3$–5) and pitch-angle anisotropy of the non-thermal electron distributions (Ramaty 1969; Fleishman and Melnikov 2003). Both optically thin and optically thick

regimes are possible. Usually the optically thin regime is realised at frequencies higher than the spectral peak of the gyrosynchrotron emission: $f > f_{\rm peak}$, and the optically thick regime at frequencies $f < f_{\rm peak}$. Note, however, that in case of relatively dense plasma, the effect of Razin suppression becomes important at low frequencies and the microwave source can be optically thin even at $f < f_{\rm peak}$. This happens quite often in observed flaring loops at frequencies $f \leq 10$ GHz (Melnikov et al. 2008).

Following the simplified expressions of Dulk (1985), the dependence of the gyrosynchrotron emission on the number of non-thermal electrons N and the magnetic field strength B is

$$I_f \propto \begin{cases} N B^{0.9\delta-0.22} & \text{in optically thin regime,} \\ B^{-0.5-0.09\delta} & \text{in optically thick regime.} \end{cases} \tag{17}$$

In the optically thin regime, the emission is very sensitive to the magnetic field in the radio source, e.g $I_f \propto B^{3.4}$ for $\delta = 4$. Thus, the modulation depth of the gyrosynchrotron emission is several times (approximately $0.9\delta - 0.22$) deeper than the relative amplitude of the magnetic field perturbation causing the modulation: the signal is amplified. For any plausible value of δ, the increase in the magnetic field increases the radio intensity in the optically thin regime and decreases it in the optically thick regime. In particular, a sausage oscillation that causes the periodic variation of the magnetic field strength, would produce anti-phase oscillations in the optically thin and optically thick parts of the gyrosynchrotron spectrum.

Similarly, consider modulation of the gyrosynchrotron emission produced by the variation of the angle between the LOS and the magnetic field,

$$I_f \propto \begin{cases} (\sin\theta)^{-0.43+0.65\delta} & \text{in optically thin regime,} \\ (\sin\theta)^{-0.36-0.06\delta} & \text{in optically thick regime.} \end{cases} \tag{18}$$

In the optically thin regime, the emission is highly dependent on the angle (for small angles), and hence variations of the angle, e.g. by a kink mode or torsional waves, are amplified by the emission mechanism. Also, again, there is the anti-correlation of the signals in the optically thin and optically thick parts of the spectrum.

In addition, in the optically thin regime, the degree of circular polarisation is

$$\rho_c \propto B^{0.78-0.55\cos\theta}, \tag{19}$$

so it increases with magnetic field, similar to the emission intensity (17), while not so strongly.

Consequently, fast magnetoacoustic waves in the microwave source can readily produce QPP. Along with this, if the emission is subject to Razin suppression, slow magnetoacoustic waves can modulate the gyrosynchrotron emission too, by the variation of the plasma density (Nakariakov and Melnikov 2006). This happens in sufficiently dense plasmas, at frequencies lower or comparable to the Razin frequency, $f_R = 2f_{\rm pe}^2/3f_{\rm ce} \approx 20\ n_0/B$, where $f_{\rm pe}$ and $f_{\rm ce}$ are electron plasma and cyclotron frequencies, respectively; in the estimating expression the electron concentration and the field are measured in cm^{-3} and G, respectively. Usually in flaring loops $f_R \leq 10$ GHz, but sometimes the Razin frequency reaches values up to 20 GHz (Melnikov et al. 2005). Under a constant magnetic field, any increase/decrease in the plasma density should lead to a subsequent decrease/increase in the emission intensity. Consequently, modulation of the plasma density by a compressible wave, e.g. a longitudinal mode, is projected onto the efficiency of Razin suppression of the gyrosynchrotron emission. At all microwave frequencies, modulation of the emission was shown to be in anti-phase with the density perturbation. The observed modulation depth can be up to an

order of magnitude higher than the perturbation of the plasma density in the wave. The modulation is more pronounced in the low frequency part of the microwave spectrum. For typical flaring loop parameters, the most suitable microwave range for the detection of slow magnetoacoustic modes was found to be 4–17 GHz, as it provides highest amplification of the modulating signal.

Thus, MHD modes of all kinds (sausage, kink, longitudinal and torsional) can modulate the microwave emission by perturbation of the parameters of the emitting plasma. MHD modes can also explain the appearance of QPP in the white light and hard X-ray emission in phase with microwave QPP, which is observed in many cases (e.g., Fig. 1). Emission in these bands is generated in the denser layers of the solar atmosphere by precipitating non-thermal electrons via bremsstrahlung. Dynamics of non-thermal electrons accelerated somewhere in the collisionless coronal part of the flaring active regions, is affected by the variations of the magnetic field in the wave. In the case of the sausage mode, this can be produced by the Zaitsev–Stepanov mechanism (Zaitsev and Stepanov 1982). A flaring loop of variable minor radius acts as a magnetic trap that confines non-thermal electrons between two magnetic mirrors situated at the loop legs. The electron dynamics is controlled by the critical pitch angle,

$$\sin^2 \alpha_c = \frac{B_{\rm top}}{B_{\rm fp}}, \tag{20}$$

determined by the ratio of the magnetic fields at the loop top, $B_{\rm top}$, and near the loop footpoint, $B_{\rm fp}$. During the acceleration/injection, the electrons with sufficiently large pitch angle $\alpha > \alpha_c$ are trapped and bounce between the magnetic mirrors created by the converging magnetic flux tube at the loop legs. The electrons with small pitch angles, within the loss-cone of the mirrors, $\alpha < \alpha_c$ escape from the trap and precipitate. Magnetoacoustic oscillations, in particular the global sausage mode, change periodically the strength of the magnetic field in the loop, varying the mirror ratio given by (20), see Fig. 6. Hence, the critical pitch angle will be periodically modulated, leading to the periodic change of the particle flux from the trap towards the loop footpoints. Reaching the lower layers of the atmosphere, the precipitated electrons interact with the dense plasma and cause hard X-ray and white

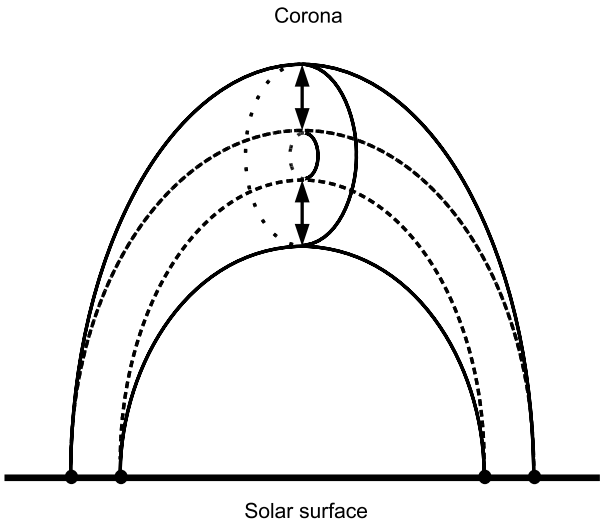

Fig. 6 The global sausage mode is a compressive mode with a wavelength of twice the loop length L. Magnetic field perturbations are maximum at the loop apex and minimum at the footpoints (from Pascoe et al. 2007)

light emission. This effect can be associated with the sausage mode and, if the plasma β is sufficiently large, with the longitudinal mode. Thus, the emission at the loop footpoints is modulated by magnetoacoustic oscillations.

Moreover, oscillating boundaries of the magnetic trap can also produce the periodic acceleration of electrons. In the trap contracting in the longitudinal direction, the electrons are subject to the Fermi acceleration, and in the transversely contracting trap to the betatron mechanism. Following Brown and Hoyng (1975), consider the consequences of betatron acceleration. Since the electron gyroradii are much smaller than the characteristic spatial scales of the magnetic trap formed by a flaring loop, the magnetic moments of an electron, $\mu = \mathcal{E}_\perp / B$, where $\mathcal{E}_\perp$ is the energy in transverse motion, is an adiabatic invariant. Hence, periodic time variations of the field result into periodic time variations in electron energy and associated QPP.

A similar mechanism was proposed by Asai et al. (2001), who considered electron acceleration by the fast shock located below the reconnection X-point in the CSHKP model of a flare. The electrons which bounce between the two slow shocks at the fast shock gain energy by a first-order Fermi process. The energy injection depends upon the length of the fast shock that is pinched by these slow shocks. If the loop situated under the reconnection site experiences transverse oscillations, the length of the fast shock can vary periodically. Consequently, the electron acceleration process should be periodic, with the period prescribed by macroscopic MHD oscillations of a loop. This effect can be produced by any fast magnetoacoustic mode, standing or propagating, and hence produced QPP can be in a rather broad range of periods.

4.5 Modulation of the Energy Release Rate by External Oscillations

MHD waves and oscillations can produce QPP by changing physical conditions not only in the emitting plasma, but also by affecting the processes of the energy release, electron acceleration and injection in the flare site. It can be achieved by either modulation of energy release rates or triggering the energy releases. As the thickness of the reconnection site is believed to be very small, even weak oscillations can produce the required modulation.

Sakai and Washimi (1982) considered the effect of incoming fast magnetoacoustic waves on tearing instability of current sheets. It was shown that the ponderomotive force due to the waves efficiently excites the plasma convection flow in the magnetic neutral sheet, which in turn enhances the tearing instability. The growth rate of the instability was found to depend upon the spatial scale of the current sheet fragmentation, the magnetic Reynolds number, the wave amplitude and the fast wave travel time across the current sheet. It is not been considered whether this mechanism can lead to appearance of QPP in the triggered flares, as it is based upon averaging of the driving wave over its period. However, perhaps, periodic wave trains can cause QPP by this mechanism.

Foullon et al. (2005) and Nakariakov et al. (2006) developed a model which explains coupling of transverse, e.g. kink or sausage, MHD oscillations in an external loop with flaring QPP (see the sketch in the left panel of Fig. 7). The external loop is situated nearby the flaring site, but is not necessarily magnetically connected to it. In the model, the MHD oscillations are not considered to be responsible for the flaring energy release itself, but play the role of its periodic triggering. According to Sect. 4.2 the period of the oscillations is determined by the size of the oscillating loop and the physical conditions in and around it. The linkage of the oscillation with the flare site is carried out by the external, evanescent or leaky, part of the oscillation. From the point of view of the flare (or, rather, pre-flare) site, this part of the oscillation is a perpendicular or oblique fast magnetoacoustic wave of,

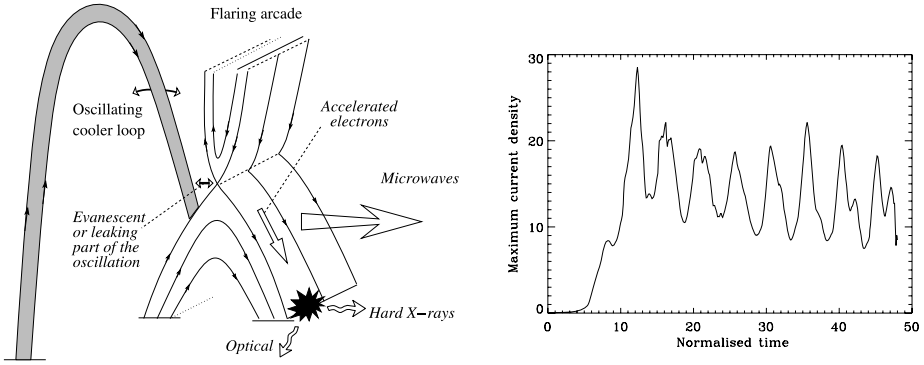

Fig. 7 *Left panel:* A sketch of the mechanism for the generation of flaring QPP by an external magnetoacoustic oscillation. The cool (*shaded*) loop experiences transverse oscillations. A segment of the oscillating loop is situated nearby a flaring arcade. An external evanescent or leaking part of the oscillation can reach magnetic null points in the arcade, inducing quasi-periodic modulations of the electric current density. The resulting current driven plasma micro-instabilities are known to cause anomalous resistivity, which triggers periodic magnetic reconnection. *Right panel:* Time evolution of the maximum electric current density in the vicinity of a 2D magnetic neutral point. The current is generated by a harmonic fast magnetoacoustic wave with the period 5 time units, coming towards the neutral point. The initial relative amplitude of the wave is 1.5%. The plasma β is finite. The normalising values are the magnetic field strength and the Alfvén speed at domain boundary, and the characteristic spatial scale of the field inhomogeneity (from Nakariakov et al. 2006)

possibly, very small amplitude, with the period prescribed by the external loop. Approaching a magnetic non-uniformity at the flare site, e.g. a magnetic X-point in the CSHKP model, the amplitude of the wave, as well as the density of the periodically varying electric current induced by the wave, increases to very large values (McLaughlin and Hood 2004).

Plasma with the current density exceeding some certain threshold value $j_{\rm thres}$, is subject to various micro instabilities which can dramatically increase the plasma resistivity. The large relative streaming between electron and ions, a consequence of the strong current density, would generate micro-turbulence that could enhance the drag between electrons and ions, producing enhanced and therefore "anomalous" resistivity. The resistivity in the plasma can then be modelled by the piecewise relation,

$$\eta = \begin{cases} \eta_{\rm class}, & \text{for } |j| \le j_{\rm thres}, \\ \eta_{\rm anom}, & \text{for } |j| > j_{\rm thres}, \end{cases} \tag{21}$$

where $\eta_{\rm class}$ and $\eta_{\rm anom} \gg \eta_{\rm class}$ are the classical and anomalous values of the resistivity, respectively. The anomalous resistivity can periodically trigger magnetic reconnection and the accompanying acceleration of charged particles. Hence, the density and energy distribution of non-thermal electrons become periodically modulated, with the period prescribed by the inducing magnetoacoustic oscillation, resulting into the periodic modulation of the X-ray, optical and radio light curves. An important feature of this mechanism is that the induced oscillations can have periods very different from the resonant periods of the flaring active region. There is no limitation on the QPP modulation depth in this model.

Foullon et al. (2005) analysed 10-min QPP in two remotely situated flares observed in hard X-rays and microwaves. The geometrical sizes of the flaring active regions could not explain the long periods of the pulsations. The observed dynamics of these two flaring sites showed a clear similarity. It was suggested that the pulsations were likely to have a common

source and be caused by kink mode oscillations in an external large loop linking the flaring sites. Indeed, such a loop, although very faint, was found in the EUV band, however it was impossible to resolve its oscillations.

A compressible wave can periodically trigger magnetic reconnection not only by periodic current density spikes, but also by the variation of the plasma density in the vicinity of the reconnection site. This possibility was modelled numerically by Chen and Priest (2006). Density variation results into a periodic variation of the electron drift speed. Depending upon the ratio of electron and proton temperatures, the value of the speed controls the onset of the Buneman or ion-acoustic instabilities and hence anomalous resistivity.

4.6 The LCR-Circuit Model

The idea that a coronal loop can be twisted and then carries an electric current gave rise to alternative mechanisms for flare-associated loop oscillations. Oscillations of the electric current in flaring loops (c.f. the torsional mode) can be represented in terms of the LCR-circuit model, developed by Zaitsev et al. (1998), see also Zaitsev and Stepanov (2008). In this model, the effective loop capacitance is determined mainly by the coronal part of the loop,

$$\mathcal{C} = \frac{c^4 \rho_0 S^2}{2\pi L I_0^2}, \tag{22}$$

where c is the speed of light, ρ_0 is the density inside the loop, I_0 is the equilibrium current and L and S are the length and cross-sectional area of the coronal part of the loop, respectively. The loop inductance is

$$\mathcal{L} = 4L\left(\log\frac{8L}{\pi a} - \frac{7}{4}\right), \tag{23}$$

where a is the minor radius of the loop, $S = \pi a^2$.

Hence, in the neglection of the electric resistance, small deviations of the electric current $\tilde{I}$ ($\ll I_0$) in the loop are described by the harmonic oscillator equation

$$\frac{1}{c^2}\mathcal{L}\frac{\mathrm{d}^2\tilde{I}}{\mathrm{d}t^2} + \frac{1}{\mathcal{C}(I_0)}\tilde{I} = 0. \tag{24}$$

The period of the electric current oscillations is

$$P_{\mathrm{LCR}} = \frac{2\pi}{c}\sqrt{\mathcal{L}\mathcal{C}}. \tag{25}$$

For typical parameters of a flaring loop, $n_e = 10^{10}$ cm^{-3}, $L = 5 \times 10^9$ cm, a practical formula for the estimation of the period is

$$P_{\mathrm{LCR}}/\mathrm{s} \approx 10 \times (I_0/10^{11})^{-1}, \tag{26}$$

where the current is measured in A.

Oscillations of the longitudinal electric current in the loop can get dissipated by e.g. Ohmic heating or other mechanisms, increasing the loop temperature and hence thermal emission from the loop. The current oscillations produce the modulation of the loop magnetic field and, therefore, gyrosynchrotron radiation of nonthermal electrons. Also, the alternate current and the associated electric field can cause periodic modulations of the energy

release rate and electron acceleration, also causing QPP of non-thermal emission. An intrinsic feature of the LCR-oscillations is their very high quality factor. The model has been applied to the interpretation of pulsations with the periods 0.7–17 s (Zaitsev et al. 1998). The pulsations with periods of ∼1 s may be observed for several minutes (see Fig. 11, right panel). All this makes the LCR approach very interesting. We would like to note, however, that the model is still under development. In particular, from the point of view of MHD wave theory, the periods of the oscillations described by LCR-contour models should be longer than the longitudinal Alfvén transit time in the loop, i.e. $P_{\rm LCR} > L/C_{A0}$. Direct comparison of the results derived from the LCR-contour model and of full MHD numerical simulations has not been performed yet.

Recent development of the LCR-contour model allowed to describe long-period parametric modulation of short-period oscillations of the current (Kislyakov et al. 2006). Consider photospheric motions in the vicinity of loop footpoints as harmonic vertical oscillations of the velocity, $\tilde{V} \propto \sin \Omega t$, with the amplitude $\tilde{V}$ and frequency Ω. The modulation of the electric current caused by the periodic footpoint driver is

$$\tilde{I} = \frac{h I_0 \tilde{V}}{\sqrt{4R^2(I_0)c^2 + \Omega^2 \mathcal{L}^2}} \sin(\Omega t - \gamma), \quad \text{and} \quad \tan\gamma = \frac{\Omega \mathcal{L}}{2R(I_0)c^2} \tag{27}$$

where I_0 is the equilibrium value of the current; $R(I_0)$ is the circuit resistance depending on the current magnitude; h is the height where the electromotive force, changing the current, acts. Thus, vertical oscillations of the loop footpoints, e.g. 5-min oscillations, can cause the corresponding modulation of the loop magnetic field and microwave emission intensity. Moreover, as the period of the oscillations in the LCR-circuit model depends upon the current in the circuit (see (22) and (25)), 5-min photospheric oscillations can cause the periodic modulation of the period of the current oscillations in the LCR-circuit model.

4.7 Ballooning and Kink Over-Stabilities

Effects of the finite plasma β and the radius of the loop's curvature provide another mechanism for generation of flaring QPP, based upon the ballooning instability. The loop curvature brings a centrifugal force, connected with the longitudinal flows of plasma along the bent magnetic field or finite plasma pressure. This force acts as an additional restoring force on transverse perturbations (e.g. kink, sausage and ballooning) if it has a component in the plane of the curvature radius. Hence, this force contributes to loop elasticity changing the resonant periods of modes (Zaitsev and Stepanov 1989).

A complete analytical theory of MHD modes of a bent magnetic cylinder has not been created yet. However, one can use estimations made for laboratory plasma devices, e.g. tokamaks. In particular, this approach brings important results for the ballooning mode (in the straight cylinder nomenclature presented in Sect. 4.1 they are the modes with $m > 2$). Consider a loop of a semi-circular shape with the major radius R, neglecting effects of gravitational stratification. Inside the loop the gas pressure is p_0 and the density is ρ_0. Suppose that the equilibrium is perturbed and there is a localised plasma perturbation, often called a plasma "tongue", with the scale $L_1 = L/n$, where $L \approx \pi R$ where n is the number of plasma tongues *along the loop* (or an integer corresponding to the longitudinal mode number, defined in Sect. 4.1).

Linear perturbations of this kind are described by the dispersion relation

$$\omega^2 - k_z^2 C_{A0}^2 = -\frac{p_0}{R\rho_0 l}; \quad \text{where } l = \begin{cases} b, & b \gg \lambda_\perp, \\ \lambda_\perp, & b \ll \lambda_\perp, \end{cases} \tag{28}$$

with $b = \rho_0 \, (\mathrm{d}\rho_0/\mathrm{d}r)^{-1}$ being the typical scale of plasma density inhomogeneity across the magnetic field in the loop and $\lambda_\perp$ is the transverse scale of plasma tongue (e.g. Stepanov et al. 2004 and references therein). Both lengths are restricted by the loop's minor radius a. We would like to point out that this approach is local, and that the potentially important effects of the external medium are here neglected. The right hand side of (28) can be also expressed through the sound speed C_{s0}.

According to Stepanov et al. (2004), the period of ballooning oscillations of a coronal loop is given by the expression

$$P_{\mathrm{ball}} \approx \frac{L}{C_{A0}} \sqrt{\frac{1}{4\,n^2 - L\beta/(2\pi l)}}. \tag{29}$$

The second term in the denominator, responsible for the ballooning effect, becomes significant for lower-n harmonics when $\beta > 2\,l/R \approx a/L$. Otherwise, (29) reduces to the expression derived in the straight cylinder approximation,

$$P_{\mathrm{ball}} \approx L/C_{A0}n, \tag{30}$$

as the RHS of dispersion relation (28) becomes negligible in this case. Expressions (29) and (30) do not take into account the effect of the external medium, which may modify the resonant period and may cause wave leakage.

Recently, Tsap et al. (2008) developed a model of kink ballooning over-stability of current-free loops, based upon the energy method. The over-stability can be excited by an imbalance between the gradients of the total pressures at the loop boundary in the vicinity of the loop apex. As the over-stability is stabilised by magnetic tension and compressibility, the most unstable perturbations correspond to the vertically polarised global kink mode which is very weakly compressible. It was found that the over-stability could be excited in loops with $\beta > 2a/R$. The period of oscillations coincides with the period of the global kink mode, and the growth time is about R/a times longer. In typical coronal loops the aspect ratio R/a is about 10–100. This estimation of the growth time does not take into account wave decay processes.

QPP of flaring emission can be produced by the ballooning over-stability by several mechanisms. For example, the development of outwardly directed tongues at the top of a loop situated under the X-point in the CSHKP model of a flare, can initiate repetitive reconnection (see Sects. 4.4 and 4.5).

5 Spatially Resolved Observations

As discussed above, there are a vast variety of mechanisms which can potentially produce flaring QPP. Different mechanisms have similar observational manifestation. This makes the identification of the specific mechanism responsible for an observed QPP event a non-trivial task. In recent years advances in microwave and hard X-ray imaging and spectroscopy have made concrete analysis of flaring QPP a more realistic possibility. The spatial information allows one to distinguish between different mechanisms responsible for the observed QPP. The crucial knowledge is the source's length morphology, the distribution of the oscillation power over the source for all detected significant periods, and phase relations between oscillations at different parts of the source in different observational bands. Mainly, all of

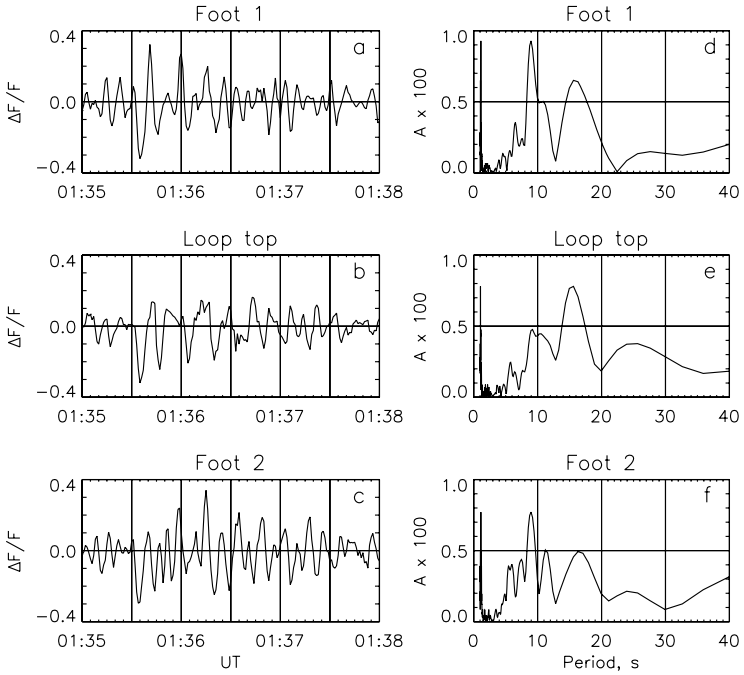

Fig. 8 The time profiles of the microwave emission at 17 GHz $\Delta F/F = [F(t) - F_0]/F_0$ normalised on the slowly varying component of the emission, F_0, obtained by smoothing the observed flux $F(t)$ over 10 s, and measured in three different regions of the size $10'' \times 10''$: the Southern (panel **a**) and Northern (**c**) legs of the loops, and the loop apex (**b**). The Fourier spectra of these time profiles are shown in panels (**d**)–(**f**), respectively. The spectra reveal that there are both the 8–11 s and 14–17 s spectral components everywhere in the loop, the shorter period component dominates at the legs (**d**) and (**f**), while the longer period component—at the apex (**e**) (from Melnikov et al. 2005)

the above is applicable to the microwave emission created by the gyrosynchrotron mechanism, as it comes from coronal structures and can be modulated by MHD oscillations (see Sect. 4.4).

Asai et al. (2001) have made first imaging microwave and hard X-ray observations of flaring QPP (a C7.9 event on 1998 November 10) using the Nobeyama Radioheliograph (NoRH) and Yohkoh hard and soft X-ray telescopes. The time resolution of NoRH is 0.1 s in flaring mode and 1 s in routine mode. The spatial resolution is $10''$ in the 17 GHz channel and $5''$ in the 34 GHz channel. The hard X-ray images were obtained with spatial and temporal resolution of about $5''$ and 0.5 s, respectively. The images allowed estimation of the size of the flaring loop and consequently the Alfvén transit time along the loop which happened to be almost equal to the period of the QPP. As a result the authors suggested, based on a shock acceleration model, that oscillations of coronal loops affect the efficiency of particle injection and acceleration. For the same flare Grechnev et al. (2003) performed a detailed analysis of the available spatial information and concluded that the period and some other properties of the microwave oscillations can be explained by MHD oscillations of the $120''$ loop connecting the sources (propagating fast or torsional waves).

The first attempt to utilise spatial information for pulsations in the case of a single flaring loop was undertaken by Nakariakov et al. (2003) and Melnikov et al. (2005) for the flare on 2000 January 12. They found that the time profiles of the microwave emission at 17 and

34 GHz exhibited quasi-periodic (with two well-detected periods $P_1 = 14$–17 s and $P_2 = 8$–11 s) variations of the intensity at different parts of the observed single flaring loop (see Fig. 8). The analysis showed the P_1 spectral component to be dominant at the top, while P_2 dominated near the footpoints of the loop (Fig. 8). The 14–17 s pulsations are synchronous at the top and in both legs of the loop. The 8–11 s pulsations at the legs are well correlated with each other but the correlation is not so obvious with the pulsations at the loop top. For this P_2 spectral component, a definite phase shift, $P_2/4 \approx 2.2$ s, between pulsations in the northern leg and loop top parts of the loop have been found. The length of the flaring loop is estimated as $L = 25$ Mm, and its average width at half intensity at 34 GHz as about 6 Mm. Microwave diagnostics shows the loop to be filled with a dense plasma with number density $n_0 \approx 10^{11}$ cm^{-3}, penetrated by the magnetic field changing from $B_0 \approx 100$ G near the loop top up to $B_0 \approx 200$ G near the north footpoint. A comparative analysis of different MHD modes of the loop demonstrates the possibility of the simultaneous existence of two modes of oscillations in the loop: the global sausage mode, with period P_1 and nodes at the footpoints, and a higher harmonic (possibly with the radial wave number $l > 1$), with P_2.

Recent analysis by Inglis et al. (2008) of an M-class event which occurred on the 1998 May 8 on the solar limb implemented more sophisticated techniques for the use of spatial information. The event was observed by NoRH and the Nobeyama Radiopolarimeter (NoRP), and by Yohkoh, SOHO and GOES satellites. QPP with the period of about 16 s were clearly observed in both microwaves and hard X-rays (see Fig. 1). In high energy bands there are two sources observed, a strong one over the southern footpoint, and a weak one at the loop top. The microwave source coincided with the X-ray flaring loop. The flaring loop length was estimated to be between 40–80 Mm. The left panel of Fig. 9 shows the distribution of the dominating period of QPP over the microwave source. The time signal of each pixel was constructed by subtracting the original signal smoothed by 50 s from the same signal smoothed by 5 s. Thus, in the constructed signal the short period (<5 s) and long period (>50 s) spectral components were suppressed. Then, the time signals of each pixel were Fourier analysed and the period of the spectral component of the highest power was determined. The distribution of those periods over the microwave source is a *periodmap* of the source. The periodmap shows that the period of about 16 s dominates in almost all pixels along the flaring loop. Thus, the microwave emission from almost all segments of the flaring loop oscillates with the same period of about 16 s.

The spatial structure of phase of the oscillations can be revealed by cross-correlation analysis. First, a pixel with the reference signal was selected, which is referred to as the "master" pixel. There is more than one possible criteria for the selection of the master pixel. For example, the master pixel can be the pixel with the highest time variance of the signal. Alternatively it may be the pixel with the highest time-integrated intensity. Once the master pixel is selected, for each other pixel of the image one can calculate the correlation coefficient between the time signal of this pixel and the time signal of the master pixel for different time lags between these signals. The central panel of Fig. 9 shows the correlation coefficient map of microwave emission, calculated with zero time lag. The pixel with the maximum value of the time integrated intensity, found near the centre of the loop emission, was chosen as the master pixel. The map shows areas with the correlation coefficient over 0.5 only. The strong correlation throughout the emitting region is evident. The right panel shows the spatial distribution of time lags between the time signal from the master pixel and other pixels, which correspond to the maximum value of the correlation coefficients. The whole emitting region appears to be strongly correlated in time with zero lag. The spatial analysis demonstrated that the QPP was consistent with the interpretation in terms of the sausage mode. However, a periodic regime of magnetic reconnection, or periodic triggering

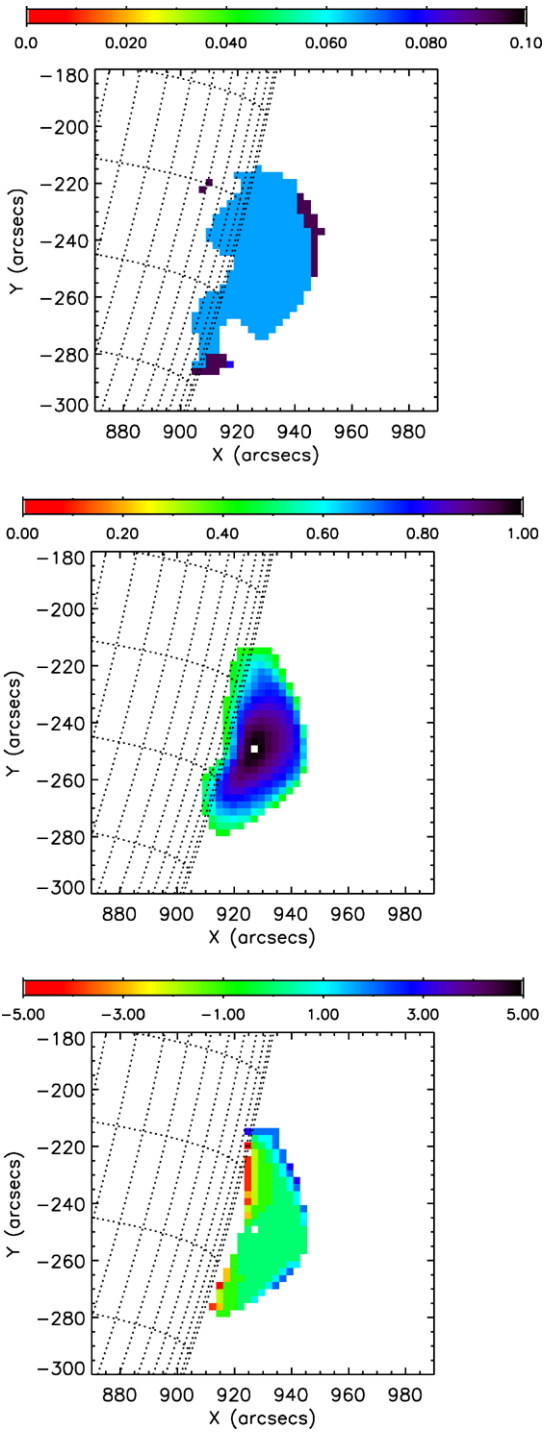

Fig. 9 *Top panel:* Periodmap of the microwave emission at 17 GHz, obtained by the Nobeyama Radioheliograph during the pulsating regime of the limb flare of 1998 May 8. *The bar* shows the colour coding of the frequencies in Hz. *Central panel:* Cross-correlation coefficient map for background subtracted. The correlation coefficient is calculated with zero time lag. The master pixel is the pixel with the highest time-integrated intensity of the signal. *The bar* shows the colour coding of the correlation coefficient. *Bottom panel:* Correlation time-lag map. *The bar* shows the colour coding of the time lag in seconds. In *the central* and *bottom panels the central white point* corresponds to the master pixel (from Inglis et al. 2008)

of reconnection by an external wave could not be ruled out. The spatial analysis reduced significantly the number of possible interpretations of the observed QPP event.

6 Multi-Periodic Pulsations

Often, spatial information on a flaring event is either incomplete or absent. In the case of stellar flaring QPP this information is absent in all cases. However, for the flares exhibiting QPP with several significant periods (e.g. Melnikov et al. 2005), the determination of the mechanism for the generation of QPP can be based on the comparative analysis of the period ratios.

Inglis and Nakariakov (2009) analysed a GOES X1.5 class event which occurred on 2002 July 3 at 02:11 UT and was observed by the Reuven Ramaty High Energy Solar Spectroscopic Imager (RHESSI), the Solar and Heliospheric Observatory (SOHO) satellites, and by NoRH and the Nobeyama Radiopolarimeter (NoRP). Light curves of this event, obtained in 17 GHz and 34 GHz channels of NoRH, 9 GHz, 17 GHz and 35 GHz bands of NoRP, and 20–40 keV and 40–60 keV energy channels of RHESSI showed pronounced QPP, which correlated well in all bands. Time spectra, e.g. periodograms, of these light curves contained several pronounced peaks. Spatially resolved analysis of the flaring oscillation was not possible on this occasion, due to instrumental problems.

Periodogram analysis is notoriously noisy, and the presence of multiple spectral peaks must be analysed with care, as they may be artificial in origin. For example, spurious strong peaks may be generated due to sidelobes and spectral leakage from a genuine strong peak. Misapplication of spectral filtering may also cause peaks to be artificially enhanced. The nature and significance of secondary peaks in a periodogram may be tested (K. Muglach, private communication). The technique is based on selective use of spectral filtering, whereby the principal peak is filtered out down to the background noise level. The periodogram is then recalculated on the remaining signal. Using this method one would expect genuine periods to increase or remain steady in spectral power, while artificial peaks would be reduced in power. This is because a strong primary peak can cause spectral leakage to other frequencies. When this primary peak is carefully removed from the signal, the recalculated periodogram confidence levels are defined as the probability of a real signal being present at the secondary frequency, given that a signal already exists at the primary frequency. This process can be iterated if there are multiple significant secondary peaks. The peaks are simply filtered in order of significance until no more peaks remain above the specified confidence level.

Figure 10 demonstrates application of this technique to the QPP event on 2002 July 3. The analysis revealed that three distinct periods were significant above 99% confidence in the microwave data, obtained with NoRH and NoRP: $P_1 \approx 28 \pm 2$ s, $P_2 \approx 18 \pm 1$ s and $P_3 \approx 12 \pm 1$ s. The 28 s and 18 s oscillations were also detected in the RHESSI light curves in the 40–60 keV energy range. The 12 s period was not detected in the X-ray flux, because of the reduced temporal resolution of the X-ray data, connected with the RHESSI spacecraft rotation which is 4 s.[3] The ratios between different periods are $P_2/P_1 \approx 0.64 \pm 0.07$ and $P_3/P_1 \approx 0.43 \pm 0.06$. If the multiple periodicity is caused by temporal harmonics of a nonlinear oscillation, because of the nonlinear doubling of frequency the resultant spectrum should be equidistant, i.e. the frequencies corresponding to different peaks are divisible by integer, and $P_2/P_1 \approx 0.5$ and $P_3/P_1 \approx 0.33$. Such a spectrum would be a characteristic feature of an aharmonic oscillation, e.g. in the oscillatory reconnection models discussed in

[3]The confident detection of the low quality oscillations requires at least 4–5 measurements per period.

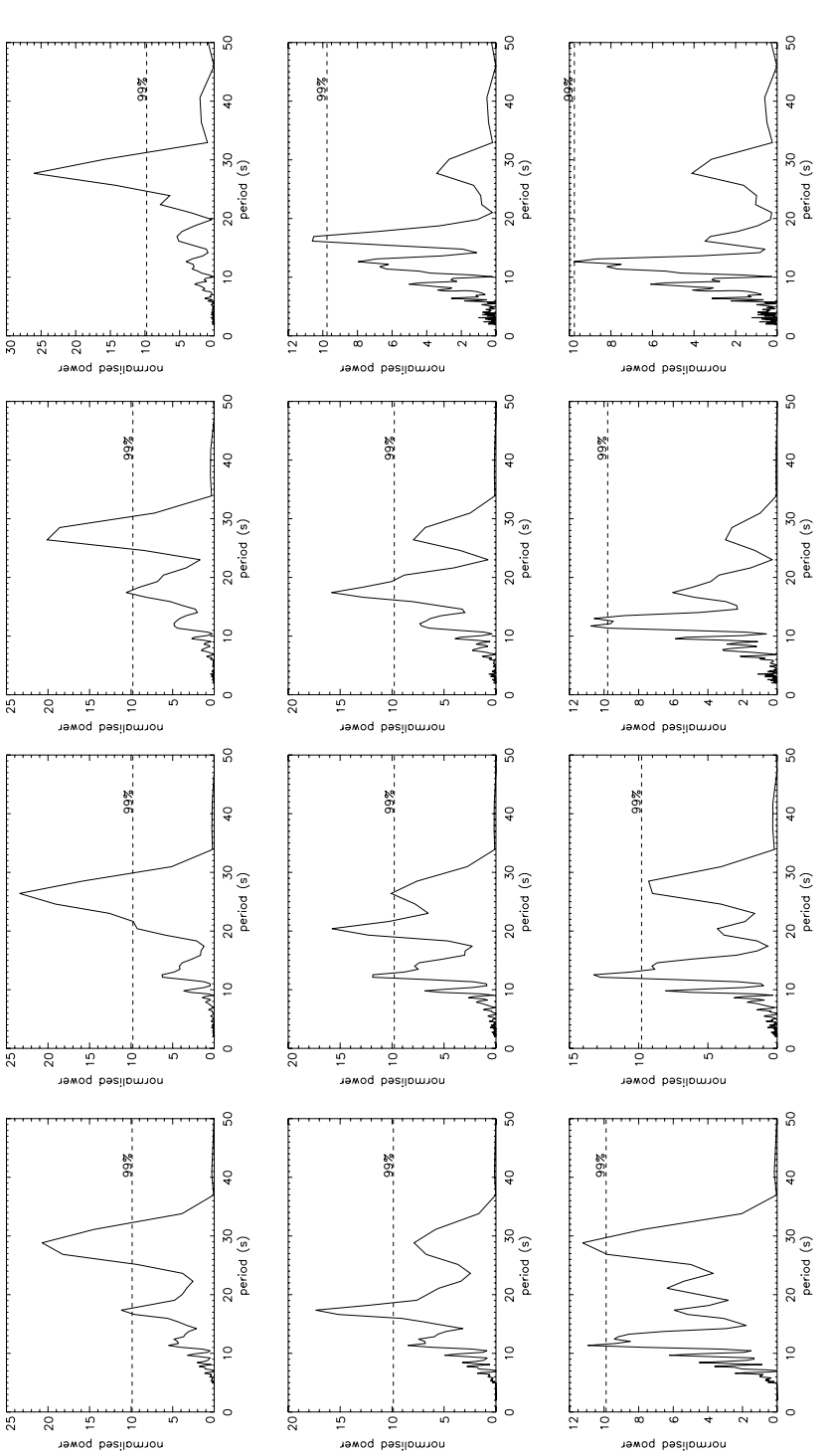

Fig. 10 Lomb–Scargle periodograms showing the effects of iterative peak suppression at different frequencies for the flaring QPP event of 2002 July 3. Columns from left to right: Nobeyama Radioheliograph data at 17 GHz and Nobeyama Radiopolarimeter data at 9 GHz, 17 GHz, 35 GHz. In all data sets the same three peaks are found above the 99% confidence level (from Inglis and Nakariakov 2009)

Sect. 2. However, the period ratios found in the data are not consistent with the $1/n$ pattern. Thus, the interpretation of the observed QPP in terms of a oscillatory regime of magnetic reconnection was ruled out.

Similar P_n/P_1 ratios appear if the frequencies are connected with different spatial MHD harmonics of a coronal loop. However, in this case the ratios deviate from the $1/n$ pattern because of dispersion (see Sect. 4.1), and the ratio becomes $P_n/P_1 = (V_1/V_n)/n$, where V_1 and V_n are the phase speeds of the global mode and the n-th harmonics, respectively. The longitudinal and torsional modes were ruled out, as they are not able to produce the observed modulations of the microwave and hard X-ray emission simultaneously. Two other modes, sausage and kink, are able to produce the observed modulation. For both sausage and kink modes, the phase speed monotonically decreases with the decrease in the wavelength, making the P_n/P_1 ratio greater than $1/n$. The observed period ratios can be rewritten as $2P_2/P_1 \approx 1.13$–1.46 and $3P_3/P_1 \approx 1.1$–1.5 which gives the monotonic decrease in the phase speed within the error bar, consistent with the theory. It was concluded that both sausage and kink modes could produce the observed QPP.

Interesting examples of linked multi-periodic oscillations were found by Kislyakov et al. (2006) in the analysis of 15 flares observed in the 37 GHz band with the Metsähovi radio telescope (Finland) with the use of the sliding window (or "windowed") Fourier transform and the Wigner–Ville nonlinear transform.[4] The telescope spatial resolution is 2.4 arc min, the sensitivity is about 0.1 sfu, and the time resolution was better than 0.1 s. During 13 events (about 90%) a 5-min periodic modulation of the emission intensity was detected with the frequency of 3.2 ± 0.37 mHz. The event and its dynamic spectrum are shown on the left panel of Fig. 11. The 5-min intensity variations are seen very clearly in both time and frequency domains. In addition, a shorter period (about 1 s) signal was detected, which was found to be frequency modulated with the same 5-min period. The short period QPP were found to be of very high quality, in contrast with the coronal loop oscillations directly observed with TRACE (see e.g. Nakariakov and Verwichte 2005). The right panel of Fig. 11 shows the light curve and both low and high frequency parts of its dynamic spectrum. The 5-min oscillations and two frequency modulated 1-s oscillations with opposite average frequency drifts are seen. The positively drifting 1-s oscillations bears a 5-min modulation, while the negatively drifting 1-s oscillation is modulated by 13.5-min signal.

Interpretation of this effect was proposed in terms of the LCR-circuit model described in Sect. 4.6. The 5-min variation of the emission intensity was associated with the modulation of the electric current in the loop by 5-min vertical photospheric motions in p-modes (see (27)). The same variation of the electric current periodically changes the LCR-circuit capacity and hence the resonant frequency of the circuit. Thus, 5-min photospheric motions were concluded to cause also periodic modulation of the short period oscillations associated with the electric current oscillations in the LCR-circuit. The simultaneous presence of the 5-min emission intensity variations and the 5-min modulation of the frequency of short period oscillations was considered as the validation of the LCR-circuit model.

[4]The Wigner–Ville transform provides a high-resolution representation in both time and frequency for non-stationary signals, however at the expense of many artefacts. By definition, it is the Fourier transform of the central covariance function of the analysed signal. The main advantage of the Wigner–Ville transform over the windowed Fourier transform is the possibility to enhance the time and frequency resolution simultaneously. The shortcomings include appearance of artefacts along both time and frequency axes, and the generation of negative energy.

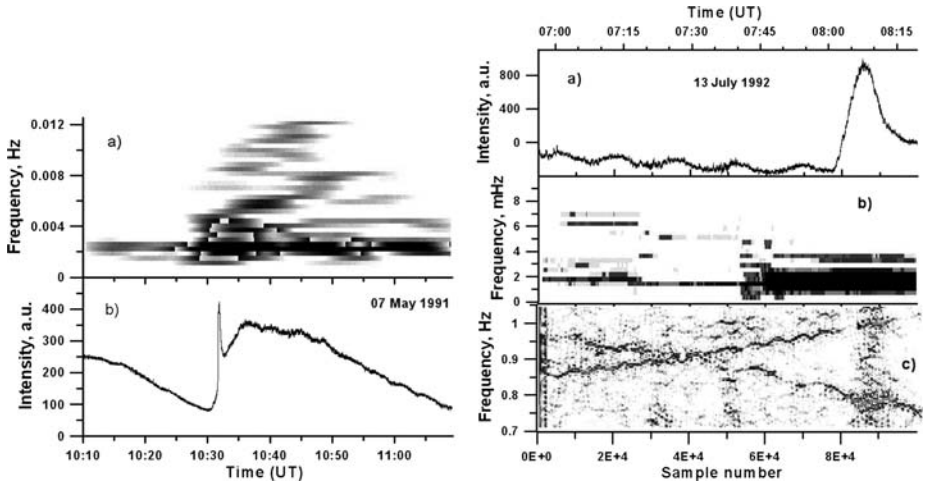

Fig. 11 *Left panel:* The light curve of microwave emission during the event of 1991 May 7 recorded with Metsähovi in 37 GHz (**b**), and the low frequency part of its dynamic spectrum (**a**). *Right panel:* The light curve of microwave emission during the event of 1992 July 13 (**a**), the low frequency part of its dynamic spectrum (**b**), and high frequency part of the same event (**c**) (from Kislyakov et al. 2006)

7 Multi-Wavelength Observations

Expressions (17)–(19), which link microwave emission generated by the gyrosynchrotron mechanism with the parameters of the emitting plasma and non-thermal electrons, can be used for the testing of the QPP generation mechanism in a specific flare (modulation of emission or particle acceleration), provided the microwave spectrum can be resolved sufficiently well. For example, observation of *anti-phase* oscillations at high, $f > f_{\rm peak}$, and low, $f < f_{\rm peak}$, frequencies could be clear evidence of gyrosynchrotron intensity modulation caused by magnetic field or viewing angle oscillations (in case of sausage mode or kink mode oscillations, respectively), as was shown to happen in the event of 1990 May 23 in which the source at low frequencies was optically thick (Qin et al. 1996; Kopylova et al. 2002).

However, in some flares the problem of choice between QPP mechanisms gets more complicated. In particular, we can not exclude the possibility of gyrosynchrotron intensity modulation by magnetic field oscillations only due to the fact that the microwave oscillations are observed to be synchronous at high and low frequencies. Oscillations may be synchronous in the case of relatively dense plasma in the gyrosynchrotron emission source, when Razin suppression becomes important.

Such a case occurred in the event of 2000 January 12 which was observed simultaneously with NoRH at 17 and 34 GHz (see Fig. 8), and with the spectrometer of the Purple Mountain Observatory (China) at the much lower frequencies 4.5–7.5 GHz (Reznikova et al. 2007). The spectral peak of the emission was determined from NoRP observations to be located at $f_{\rm peak} \approx 9$ GHz. The wavelet[5] power spectra of the QPP at 4.5 GHz and 34 GHz are shown

[5]The main advantage of the wavelet transform over the windowed Fourier transform is the automatic adjustment of the window function according to the examined frequency, see http://atoc.colorado.edu/research/wavelets/.

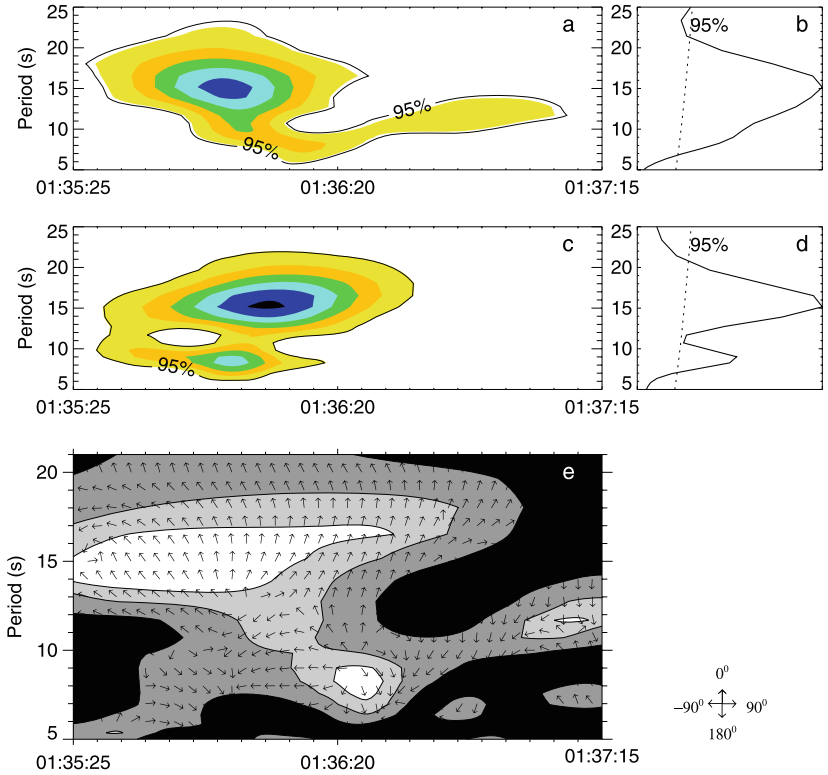

Fig. 12 The multi-wavelength analysis of the event on 2000 January 12 observed by the spectrometer of the Purple Mountain Observatory at 4.5 GHz and by the Nobeyama Radio Observatory at 34 GHz. (**a**) Wavelet power spectrum (using the Morlet wavelet) of 4.5 GHz flux variations. (**c**) Same as (**a**) but for 34 GHz. (**b**) and (**d**) The corresponding global wavelet spectra. The 95% confidence level is shown by the solid black contour in (**a**), (**c**) and by *dotted line* in (**b**), (**d**). (**e**) The wavelet coherency and phase between flux variations at 4.5 GHz and 34 GHz. *Black*, *dark grey*, *grey* and *white colours* are for wavelet squared coherencies greater 0, 0.5, 0.8, and 0.9, respectively. The phase difference is indicated by vectors (see the key on the right side) (from Reznikova et al. 2007)

in Fig. 12(a) and (c), respectively. It is seen that both of the analysed signals contain well-pronounced periodicity with the average period of $P = 15$ s during the impulsive phase of the burst. To get an idea about the synchronism the wavelet coherency between microwave pulsations at 4.5 GHz and 34 GHz is shown in Fig. 12(e). The vectors in Fig. 12(e) indicate the phase difference between 4.5 GHz and 34 GHz flux variations at the time-period plane (see key at the right side). As follows from Fig. 12(e), the region with high coherency (>0.9) for 14–16 s component shows the stable in-phase behaviour (vectors directed upward).

The most interesting result of this analysis is that the pulsations with period of 14–16 s observed at the Purple Mountain Observatory, China and NoRH frequencies are synchronous with each other. In the studies of Nakariakov et al. (2003), Melnikov et al. (2005) similar periodicity at high frequencies was confidently interpreted in terms of the global sausage mode oscillation of the magnetic tube. Radio diagnostics has shown the following values of averaged magnetic field and plasma density in the flaring loop: $B_0 = 120$ G, $n_0 = 8 \times 10^{10}$ cm^{-3}. The corresponding value of Razin frequency is $f_R \approx 13$ GHz. Under such conditions, the emission source at low frequencies $f < f_{peak}$ becomes optically thin

due to Razin suppression, and, therefore, oscillations have to be synchronous with pulsations at high frequencies $f > f_{\rm peak}$. Using the above values of B_0 and n_0, and assuming that their disturbances are produced by the global sausage mode oscillations, Reznikova et al. (2007) have modelled time profiles of the modulation depth at various observed frequencies and obtained a good agreement with the observed modulation depths.

Another interesting flare, which also produced in-phase QPP at low and high frequencies, was studied in detail by Fleishman et al. (2008). Various multi-wavelength spectral information on this flare was applied for distinguishing between two mechanisms for generation of QPP: the modulation of microwave emission by MHD oscillations of the flaring loop and quasi-periodic injection or acceleration of non-thermal electrons. The GOES X1.3 flare occurred near the limb on 2003 June 15 and was simultaneously observed by both the Owens Valley Solar Array (OVSA) and Nobeyama radio telescopes NoRH and NoRP. In addition, the flare was observed in hard X-rays by RHESSI. A single SOHO EIT 195 Å image was available too. OVSA typically observes 40 frequency channels distributed logarithmically over the frequency range 1–18 GHz, providing the microwave spectral resolution. Using spectral and spatial information the authors determined that the microwave source was optically thick at low frequencies $f < f_{\rm peak} \approx 10$ GHz, and Razin suppression was unimportant. The corresponding Fourier analysis showed that the observed QPP were multi-periodic. The two most significant spectral peaks in the signals recorded at high frequencies of 17 and 35 GHz (in the optically thin regime) correspond to periods of 14.5 and 18.4 s. The phase of main Fourier peaks showed phase coherence over the whole frequency range, including low (optically thick) frequencies. At the same time, the phase of the dominant Fourier peak varied systematically from high to low frequencies, corresponding to a relative timing delay between signals at different frequencies. Examination of the modulation of the degree of circular polarisation and of the radio spectral index showed anti-phase behaviour with the modulation of the emission flux. The observed properties of the oscillations were compared with those derived from two simple models for the radio emission, one considering MHD oscillations, and another the quasi-periodic injection of fast electrons.

Fleishman et al. (2008) concluded that the detailed spectral information available for the analysed event did not make possible a consistent fit to the data within the MHD oscillation model. By comparison, the model with quasi-periodic particle injection (without its specification) was claimed to fit excellently to the variations in microwave flux density, power-law index, and polarisation, as well as their correlations with each other and with hard X-ray QPP. This was found to be applicable to all significant periods detected in the signal. What mechanisms could be responsible for such a quasi-periodic particle injection? One of the options could be a periodic regime of magnetic reconnection, which would periodically generate non-thermal electrons. But, as discussed in Sects. 2 and 6, multi-periodic regimes of magnetic reconnection are not known. Thus, the results obtained by Fleishman et al. (2008) seem to be consistent with the model linking QPP with modulation of the energy release rate by external multi-modal oscillations, discussed in Sect. 4.5.

8 Conclusions

Exploitation of the valuable seismological potential of flaring QPP, i.e. the diagnostics of physical conditions in flaring regions and processes operating in them, requires correct identification of the physical mechanisms generating the pulsations. There are two main groups of suitable mechanisms for the generation of long period QPP: MHD oscillations and waves in or near flaring magnetic structures, and repetitive regimes of magnetic reconnection and

of non-thermal particle acceleration. Generally, all known types of MHD oscillations can induce QPP with parameters (periods and their ratios, evolution, signatures, quality, modulation depth, spectral information) which contain information for plasma diagnostics. Oscillatory magnetic reconnection, in turn, can also be described as an MHD auto-oscillation or auto-wave. It is quite likely that different QPP events are caused by different mechanisms or even their combination. For example, long period energy releases can excite natural oscillations in various MHD resonators in the vicinity of the flaring epicentre, which in turn modulate subsequent energy releases. Identification of those mechanisms would impose additional constrains on MHD wave plasma diagnostics, and hence reduce its ambiguity.

Despite significant progress in both theoretical and observational aspects of the study of coronal MHD wave, magnetic reconnection and flaring energy release, the available observational information and theoretical modelling are in the majority of cases insufficient for the confident identification of the physical mechanisms responsible for QPP. However, the multi-wavelength, broadband, multi-periodic approaches reviewed above and their synthesis clearly demonstrate the promising approach to this problem. Spatial resolution gives the distribution of the phase and amplitude of the QPP over the emission source, allowing for the determination of the MHD mode type. Techniques of periodmapping, coherence and correlation mapping seem to have great potential and require further development. Valuable information can also be obtained from QPP events with several significant periodicities. The period ratios are determined by the QPP generation mechanism, and thus help to identify the physical mechanism. Even more useful could be spatially resolving observations of multi-periodic QPP events, when different parts of the source have different periods. Important information is also contained in the phase and amplitude relations between QPP measured at different microwave frequencies, e.g. when QPP are observed simultaneously in optically thin and thick regimes.

Further progress requires dedicated multi-wavelength multi-instrumental investigation of flaring QPP events, as well as advancing the relevant theory and data analysis techniques. The vast abundance and variety of observational examples of flaring QPP require the development of a cataloguing system, utilising phenomenologically determined parameters of QPP, hosting flares and, when available, morphology and geometry of flaring active regions. Some important theoretical topics are also in the embryonal state at the moment, e.g. the study of MHD wave interaction with the processes of magnetic reconnection, energy release and particle acceleration. It is clearly one of the important future avenues in coronal physics, which can shed light on the flare energetics and triggering. Also, the process of the excitation of MHD waves by energy release processes and possible contribution of the waves in electron acceleration directly or through the generation of plasma turbulence is an interesting issue, as it could be an important ingredient of the flare energetics.

The study of flaring QPP has also multi-disciplinary implications: e.g. in stellar astrophysics it opens up unique perspectives for stellar MHD coronal seismology, is directly relevant to Earth's and planetary magnetospheric seismology, and may be of interest for MHD spectroscopy of laboratory plasmas. All this makes the study of flaring QPP an important, interesting and timely research topic.

Acknowledgements This review is based upon the discussions with the members of the Science Team "Coronal waves and oscillations" at the workshop at ISSI, Bern, Switzerland, and was also supported by the Royal Society British–Russian Research Collaboration grant, and (VM) by the RFBR grants No 07-02-01066, 08-02-92228, 09-02-00624.

References

A. Asai, M. Shimojo, H. Isobe, T. Morimoto, T. Yokoyama, K. Shibasaki, H. Nakajima, Astrophys. J. **562**, L103 (2001)

M.J. Aschwanden, Solar Phys. **111**, 113 (1987)

M.J. Aschwanden, in *Turbulence, Waves and Instabilities in the Solar Plasma*, ed. by R. Erdelyi, K. Petrovay, B. Roberts, M.J. Aschwanden. NATO Science Series II: Mathematics, Physics and Chemistry, vol. 124 (Kluwer Academic, Dordrecht, 2003), p. 215

M.J. Aschwanden, in *SOHO 15 Coronal Heating*, ed. by R.W. Walsh, J. Ireland, D. Danesy, B. Fleck. ESA SP-575 (2004), p. 97

M.J. Aschwanden, A.O. Benz, Astrophys. J. **332**, 466 (1988)

D. Banerjee, R. Erdélyi, R. Oliver, E. O'Shea, Solar Phys. **246**, 3 (2007)

J.C. Brown, P. Hoyng, Astrophys. J. **200**, 734 (1975)

P.F. Chen, E.R. Priest, Solar Phys. **238**, 313 (2006)

G.A. Dulk, Ann. Rev. Astron. Astrophys. **23**, 169 (1985)

P.M. Edwin, B. Roberts, Solar Phys. **88**, 179 (1983)

R. Erdélyi, I. Ballai, Astron. Nachr. **328**, 726 (2007)

G.D. Fleishman, Q.J. Fu, G.-L. Huang, V.F. Melnikov, M. Wang, Astron. Astrophys. **385**, 671 (2002)

G.D. Fleishman, T.S. Bastian, D.E. Gary, Astrophys. J. **684**, 1433 (2008)

G.D. Fleishman, V.F. Melnikov, Astrophys. J. **584**, 823 (2003)

C. Foullon, E. Verwichte, V.M. Nakariakov, L. Fletcher, Astron. Astrophys. **440**, L59 (2005)

V.V. Grechnev, S.M. White, M.R. Kundu, Astrophys. J. **588**, 1163 (2003)

P.C. Grigis, A.O. Benz, Astron. Astrophys. **426**, 1093 (2004)

J. Heyvaerts, E.R. Priest, D.M. Rust, Astrophys. J. **216**, 123 (1977)

A.R. Inglis, V.M. Nakariakov, Astron. Astrophys. **493**, 259 (2009)

A.R. Inglis, V.M. Nakariakov, V.F. Melnikov, Astron. Astrophys. **487**, 1147 (2008)

S.R. Kane, K. Kai, T. Kosugi, S. Enome, P.B. Landecker, D.L. McKenzie, Astrophys. J. **271**, 376 (1983)

A.G. Kislyakov, V.V. Zaitsev, A.V. Stepanov, S. Urpo, Solar Phys. **233**, 89 (2006)

B. Kliem, M. Karlický, A.O. Benz, Astron. Astrophys. **360**, 715 (2000)

Y.G. Kopylova, A.V. Stepanov, Y.T. Tsap, Astron. Lett. **28**, 783 (2002)

N.P.M. Kuin, P.C.H. Martens, Astron. Astrophys. **108**, L1 (1982)

J.A. McLaughlin, A.W. Hood, Astron. Astrophys. **420**, 1129 (2004)

M. Mathioudakis, J.H. Seiradakis, D.R. Williams, S. Avgoloupis, D.S. Bloomfield, R.T.J. McAteer, Astron. Astrophys. **403**, 1101 (2003)

V.F. Melnikov, D.E. Gary, G.M. Nita, Solar Phys. **253**, 43 (2008)

V.F. Melnikov, A. Magun, Solar Phys. **178**, 153 (1998)

V.F. Melnikov, V.E. Reznikova, K. Shibasaki, V.M. Nakariakov, Astron. Astrophys. **439**, 727 (2005)

U. Mitra-Kraev, L.K. Harra, D.R. Williams, E. Kraev, Astron. Astrophys. **436**, 1041 (2005)

D.A.N. Müller, H. Peter, V.H. Hansteen, Astron. Astrophys. **424**, 289 (2004)

M.J. Murray, L. van Driel-Gesztelyi, D. Baker, Astron. Astrophys. **494**, 329 (2009)

V.M. Nakariakov, Adv. Space Res. **39**, 1804 (2007)

V.M. Nakariakov, T.D. Arber, C.E. Ault, A.C. Katsiyannis, D.R. Williams, F.P. Keenan, Mon. Not. R. Astron. Soc. **349**, 705 (2004)

V.M. Nakariakov, C. Foullon, E. Verwichte, N.P. Young, Astron. Astrophys. **452**, 343 (2006)

V.M. Nakariakov, V.F. Melnikov, Astron. Astrophys. **446**, 1151 (2006)

V.M. Nakariakov, V.F. Melnikov, V.E. Reznikova, Astron. Astrophys. **412**, L7 (2003)

V.M. Nakariakov, D.J. Pascoe, T.D. Arber, Space Sci. Rev. **121**, 115 (2005)

V.M. Nakariakov, D. Tsiklauri, A. Kelly, T.D. Arber, M.J. Aschwanden, Astron. Astrophys. **414**, L25 (2004)

V.M. Nakariakov, E. Verwichte, Living Rev. Sol. Phys. **2**, 3 (2005)

L. Ofman, L. Sui, Astrophys. J. **644**, L149 (2006)

D.J. Pascoe, V.M. Nakariakov, T.D. Arber, Astron. Astrophys. **461**, 1149 (2007)

Z. Qin, C. Li, Q. Fu, Z. Gao, Solar Phys. **163**, 383 (1996)

R. Ramaty, Astrophys. J. **158**, 753 (1969)

V.E. Reznikova, V.F. Melnikov, Y. Su, G. Huang, Astron. Rep. **51**, 588 (2007)

B. Roberts, P.M. Edwin, A.O. Benz, Astrophys. J. **279**, 857 (1984)

J.-I. Sakai, H. Washimi, Astrophys. J. **258**, 823 (1982)

K. Shibasaki, Astrophys. J. **557**, 326 (2001)

A.V. Stepanov, Y.G. Kopylova, Y.T. Tsap, K. Shibasaki, V.F. Melnikov, T.B. Goldvarg, Astron. Lett. **30**, 480 (2004)

T. Tajima, J. Sakai, H. Nakajima, T. Kosugi, F. Brunel, M.R. Kundu, Astrophys. J. **321**, 1031 (1987)

B. Tan, Solar Phys. **253**, 117 (2008)

Y.T. Tsap, Y.G. Kopylova, A.V. Stepanov, V.F. Melnikov, K. Shibasaki, Solar Phys. **253**, 161 (2008)
D. Tsiklauri, V.M. Nakariakov, T.D. Arber, M.J. Aschwanden, Astron. Astrophys. **422**, 351 (2004)
T. Van Doorsselaere, A. Debosscher, J. Andries, S. Poedts, Astron. Astrophys. **424**, 1065 (2004)
V.V. Zaitsev, Solar Phys. **20**, 95 (1971)
V.V. Zaitsev, A.V. Stepanov, Issled. Geomagn. Aeron. Fiz. Solntsa **37**, 3 (1975)
V.V. Zaitsev, A.V. Stepanov, Sov. Astron. Lett. **8**, 132 (1982)
V.V. Zaitsev, A.V. Stepanov, Sov. Astron. Lett. **15**, 66 (1989)
V.V. Zaitsev, A.V. Stepanov, Phys. Uspekhi **51**, 1123 (2008)
V.V. Zaitsev, A.V. Stepanov, S. Urpo, S. Pohjolainen, Astron. Astrophys. **337**, 887 (1998)